THE PRODUCTION OF HIGH INTENSITY PROTON BEAMS

Thesis by

Robert Noel Hall

In Partial Fulfillment of the Requirements

For the Degree of

Doctor of Philosophy

California Institute of Technology

Pasadena, California

1948

ACKNOWLEDGEMENT

The author is indebted to Professor C.C. Lauritsen for many helpful suggestions concerning all phases of the work described in this paper. Dr. Fowler supervised the measurement of the carbon cross-section, and both he and Dr. Christy contributed to the interpretation of the results. Dr. T. Lauritsen helped in many ways in the development of the ion source.

A pre-doctoral fellowship from the National Research Council enabled the author to pursue his graduate studies. The work described in this paper was carried on under contract with the Office of Naval Research.

ABSTRACT

A high frequency ion source was developed for use in constant voltage accelerators. Analyzed proton beams of several hundred microamperes were produced in a 130 kv accelerating system designed to simulate the initial sections of a high voltage accelerator.

The focusing properties of constant voltage accelerating systems are discussed, including the effects of space-charge in the initial accelerating electrodes. The focal properties of multicylinder accelerating columns are calculated.

The high intensity proton beam produced by the ion source and 130 kv accelerator was used to investigate the $C^{12}(p,\gamma)N^{13}$ reaction, which is of importance in the understanding of stellar phenomena. A cross-section of 1.5×10^{-34} cm^2 was measured at bombarding energies of 100 kev.

CONTENTS

CONTENTS - Continued

ILLUSTRATIONS

Fig.

I. INTRODUCTION

The Production of Proton Beams

Electrostatic accelerators are used extensively at present in the investigation of nuclear reactions at energies up to about five million electron volts, using protons or deuterons as bombarding particles. While magnetic resonance devices such as cyclotrons are able to produce more intense beams than have been attained with constant voltage accelerators, the emerging particles are neither well collimated nor monoenergetic, and are accompanied by an intense radiation background. On the other hand, electrostatic accelerators and transformer-condenser outfits generally produce beams less than a few millimeters in diameter, with roughly a kilovolt of energy spread, and with a background comparable to that of cosmic rays. The useful beam current, however, is often limited to a few microamperes which is inadequate for the study of many reactions. Greater intensity would simplify considerably many investigations, and would permit more effective use of the measuring equipment.

This paper describes some work which has been done on the problem of increasing the useful beam current of constant voltage accelerators. A new ion source was

developed in experimental investigations using a low-voltage accelerator which simulated, as far as possible, the conditions encountered in high-voltage equipment. The optical properties of the accelerating system are discussed in order that an ion beam having the desired characteristics might be produced. Since hydrogen and deuterium behave similarly, the discussion will be generally restricted to the production of proton beams.

Components of the Constant Voltage Accelerator

We are concerned with three parts of the accelerator which may be studied separately: the ion source, the ion gun, and the accelerating column. (See Fig. 1)

The ion source generates the ions at energies of a few electron volts in the neighborhood of a small exit hole whose function is to reduce the flow of hydrogen, and to define a small area which will be imaged upon the target by the accelerating system. As the ions emerge from the opening, they are accelerated and focused by the initial electrodes, the "ion gun", into a beam of about fifty kilovolts energy. This ion gun is responsible for most of the characteristics of the resulting beam. The subsequent accelerating electrodes serve to raise the energy of the ions to the desired bombarding energy, but usually produce very little focusing effect.

Requirements of the Accelerating System

The beam, in passing down the column, must not produce conditions which lead to electrical breakdown. The gas pressure in the accelerating column can be easily maintained at a value below the sparking pressure of approximately 10^{-4} millimeters of mercury. It is believed[1,2,3] that breakdown is the result of excessive electrode bombardment by stray ions which produces secondary electrons and releases adsorbed gases. These secondaries, in turn, produce more stray ions and this cumulative process results in a discharge. The stray ions which initiate this process arise largely from collisions of focused ions with residual gas molecules. On the basis of this mechanism, it follows that higher proton currents may be tolerated if the gas pressure is reduced, or if the beam current, not due to protons, is reduced.

The gas pressure in the column is mainly determined by the rate of gas flow into the column and by its pumping speed. The gas flow into the column may be substantially reduced if a differential pumping arrangement is provided between the exit hole in the ion source and the first electrode of the ion gun. This gas flow is again reduced if the efficiency of the source is made as high as possible. This efficiency, defined as the ratio of

the number of protons focused upon the target to hydrogen molecules consumed by the ion source per unit time, is usually of the order of 10^{-3}. At this efficiency, a 100 microampere proton beam corresponds to a gas flow of 84 cc per hour of hydrogen at atmospheric pressure.

The beam consists essentially of three kinds of ions: protons, singly charged hydrogen molecules, and molecules to which a proton has been added. The mass two and mass three components are less frequently used, and are detrimental in that they constitute an undesirable load upon the high voltage generator and contribute to the formation of stray ions as well as space-charge spreading of the beam.

In addition to delivering a copious supply of protons, accompanied by a relatively small flow of hydrogen and mass two and three ions, it is essential that the ion source have a long life. Simplicity of construction and operation is also highly desirable.

The accelerating system may be regarded as a compound lens system whose function is to produce a nearly parallel ion beam of small diameter which images the exit hole at a point on, or near, the target. The focal length of the equivalent single lens determines the size of the image and the convergence of the rays which form it. The properties of a wide variety of electrostatic

lenses are now known[4,5] so that the ion gun may be designed to produce the desired beam characteristics. In addition to its lens action, the gun serves as an aperture stop to remove widely diverging ions which would strike the accelerating electrodes, or which would not focus well because of the aberrations of the lenses.

Space-charge effects complicate the picture but may be accounted for in many cases. In general, the effects are negligible except in the gun, where the beam has low energy, and in cases where the beam must pass through a long drift tube before reaching the target.

High voltage accelerating columns of reasonable length are necessarily constructed of alternate layers of insulator and conductor. Since the column must have a high pumping speed, the accelerating electrodes are generally short and have a large inside diameter. The resulting accelerating field is very nearly uniform, and even the initial accelerating gaps of the column produce very little focusing action, as will be shown in Chapter VI.

There are many considerations involved in producing intense beams of high energy protons. It is hoped that the following discussion will serve to clarify the problem and to indicate progress which has been made in certain phases of it.

II. EQUIPMENT

Accelerating Column

In order that the results of this investigation might most readily be used in the new electrostatic accelerator under construction at the California Institute, the accelerating column used for the ion source investigation was constructed largely of components of the new accelerator. This column is shown in Figs. 2 and 3. There are four accelerating gaps, of which the first three will be regarded as constituting the ion gun, while the fourth corresponds to the first gap in the accelerating column proper.

The column is assembled as a unit and is attached to the vacuum manifold in a horizontal position by four porcelain rods. Corona rings surround the column to reduce sparking which would otherwise limit the voltage. A photograph of the completely assembled column mounted in position is shown in Fig. 4. Figure 5 shows a plan view of the essential components of the entire system.

Vacuum System

The main vacuum is provided by an 8", two-stage, oil diffusion pump which attains a pressure of 2×10^{-5} mm Hg as measured by the ion gage when there is no hydrogen flow. A 2" oil pump is used to remove hydrogen

from the first gap of the ion gun. This pump is at ground potential and is connected to the column by a section of glass tubing.

A pirani gage, mounted in the fore-pump side of the 2" oil pump, is used to measure the rate of flow of hydrogen. Closing a valve between the fore-pump and the 2" pump causes the pressure on the fore-pump side of the latter to rise at a measurable rate until its pumping action ceases. Knowledge of the rate of rise of pressure and the volume into which the hydrogen is compressed permits a reasonable estimate of the rate of hydrogen flow.

High Voltage Supply

A high voltage X-ray tube power supply capable of delivering a current of several milliamperes at a voltage of 115 kv produces most of the accelerating potential. The voltage is measured by a resistor stack consisting of 100 one megohm wire-wound resistors in series with a 20 megohm resistor. These resistors were compared with a 20 megohm precision resistor and all were found to agree with their nominal values within a few tenths of one per cent. The current was measured by a Simpson meter calibrated at intervals by a Rawson Type 501 milliammeter which, in turn, was calibrated by Mr. J. N. Harris of the Calibration Laboratory. The Simpson meter

was found to retain its calibration quite accurately. It is believed that the voltage measurements are accurate to within one per cent.

The ripple from the high voltage supply was checked on an oscilloscope at voltages up to 50 kv using a blocking condenser. Extrapolation to 115 kv indicates that at this voltage the ripple is approximately 2 kv peak-to-peak.

Ion Source Supplies

A large aluminum box, mounted on insulators, houses a 115 volt, 60 cycle generator and the power packs required to run the ion source. The generator is turned through a belt drive by a 1 hp motor.

The ion source consists of an electrodeless radio frequency discharge in a strong magnetic field. Four 8025A high frequency triodes, mounted in a cavity resonator, supply 60 watts at 450 mc/sec. An electromagnet, driven by a low voltage rectifier, produces a magnetic field of up to 2500 gauss inside the discharge chamber.

The voltage across the first accelerating gap is obtained from a 15 kv rectifier whose output is arranged so that it adds to the main accelerating voltage, thus producing a total accelerating potential of 130 kv. The first accelerating electrode serves as an aperture stop to prevent stray ions from being sent down the column.

The current collected by this electrode is never over 2 ma, but is more than can be handled by corona gaps which are adequate for the control of the other electrodes.

The usual palladium thimble and nichrome heater arrangement is used to control the flow of hydrogen through the ion source.

Ion Current Measurement

Magnetic analysis is employed to separate the various beam components. The component to be measured is deflected through an 18° angle and is collected by a Faraday cage placed 16" beyond the magnet. A typical analysis curve is shown in Fig. 6. The heights of the mass two and three peaks are proportional to the number of charges in the beam, and must be multiplied by two and three respectively to represent the abundance of half-energy and one-third energy protons in the beam. The guard ring of the Faraday cage is well shielded from the beam and its voltage was adjusted so as to be well above the value required to return all secondary electrons. The calibration of the current meter was checked with the meter mounted in place.

The current collector, shown in Fig. 7, was designed to serve as a target holder for the study of low voltage proton reactions with C^{12} and N^{14}. The targets are

supported on a water-cooled sphere which may be rotated 180° in order that the positron radioactivity resulting from the bombardment may be measured by a mica window beta-ray counter.

III. ION SOURCE

Summary of Ion Source Development

Early ion sources[6,7] employed a cold cathode, high voltage (40 kv) hydrogen discharge to create the ions which escaped from the discharge chamber through an opening, or canal, in the cathode. (See Fig. 8a) The canal reduced the gas flow and helped direct the ions down the accelerating tube. Beam currents produced in this manner were rather small and the high energy ions from the discharge rapidly eroded the canal. Moreover, the ions emerged from the canal with a large distribution in energy which made them difficult to focus, and prohibited their use in high resolution nuclear investigations.

Crane, Lauritsen, and Soltan[8] describe an ion source in which electrons from a hot cathode are accelerated by an anode at a potential of 1000 volts and produce ionization in hydrogen at a pressure of 10^{-3} mm Hg. A probe which contains the canal is maintained at a negative potential of 2500 volts to draw the ions out of the discharge.

Since 1933[9], low voltage are discharge sources have been extensively developed and are in general use today in a variety of forms, as illustrated in Fig. 8b. Each

form employs an arc discharge at a pressure of a few tenths of a millimeter of mercury in the neighborhood of a small hole through which the ions escape. In one form[1,2,10], the arc passes through a glass or metal capillary, a few millimeters in diameter, which is perpendicular to the axis of the accelerator, the exit hole being in the side of the capillary. In another form, known as the Zinn source[11,12], the anode is surrounded by a constricting nozzle which, in turn, is within a ring-shaped cathode, all three being coaxial with the accelerator. Both modifications have been used frequently with a negative probe immediately beyond the exit hole in an effort to increase the yield. It was the author's experience that, in the case of a Zinn source, greater yields were obtained by removing the probe and letting the ions diffuse out of the exit hole and into an accelerating field. Similar results have been reported[1,2] for capillary arc sources.

In a third type of low voltage arc source, developed at Carnegie Institution of Washington[13], the discharge is not constricted but, instead, a negative probe is inserted into the discharge chamber to extract the ions.

Low voltage arc sources generally do not produce a very large fraction of mass one ions (protons), and high currents are obtained only with a severe reduction in

cathode life. The use of a probe introduces an energy spread among the ions equal to the probe voltage.

Some ion sources recently developed yield high proton fractions and operate at relatively low pressures. These sources, shown in Fig. 8c, make use of an axial magnetic field to restrict the motions of the charged particles of the discharge.

In 1940, Finkelstein[14] described an ion source in which electrons oscillate between the cathode and the exit hole, being constrained to the axis of the system by a magnetic field. In their oscillations, the electrons travel a considerable distance before being collected. Accordingly, a moderate emission of electrons by the cathode, in the presence of low pressure hydrogen, maintains a large current flow of oscillating electrons which strongly ionizes the hydrogen. Since the hydrogen pressure is only about .01 mm Hg, the exit hole may be made a few millimeters in diameter without excessive gas flow, and considerable ion current may be obtained. This source was used successfully by Von Ardenne[15], who obtained a 1 Mev beam containing 50 μa of protons. Gas consumption is very low, amounting to as little as 100 H_2 molecules per proton. A similar arrangement is being developed at Imperial College in Britain[16], where a discharge is maintained between two cold cathodes in a

magnetic field by a ring anode between them. The Finkelstein source has a somewhat limited cathode life, and the British source uses a rather high anode voltage which introduces a spread in ion energy. Both employ a large exit hole which tends to produce a large focused image upon the target.

High frequency electrodeless discharges have been used recently as ion sources. The absence of electrodes would indicate long life, and the high frequency field would contribute negligible energy to the ions formed in the discharge. Moreover, one might hope to attain strong discharges at relatively low pressures because the ions and electrons in the discharge travel through a large distance in their oscillatory motion before colliding with the walls of the vessel.

High frequency sources developed in Britain[16,17] use up to 100 watts of 60 to 180 mc/sec power dissipated in pyrex vessels of about 200 cc volume. A negative probe, inserted into the discharge at a potential of one or two kilovolts with respect to the plasma, causes the plasma to recede from it. The roughly spherical boundary thus formed tends to focus the ions upon the exit hole in the probe. An axial magnetic field greatly augments the ion yield. It is found that the proton current passes through a maximum at a certain magnetic field strength,

40 gauss for 60 mc/sec excitation frequency, and 130 gauss for 180 mc/sec R.F. The pressure in the discharge is very low (.01 mm Hg), so that even with the 3 mm exit holes employed the gas flow is only about 10 cc per hour. The high voltage probe probably introduces a considerable energy spread among the ions, and also gives them a large transverse velocity which complicates the focusing problem.

The similarity of the Finkelstein source and the British radio frequency sources is worth pointing out. In each case, the ionization is caused by particles oscillating along a magnetic field in a gas pressure of .01 mm Hg. The exit hole is several millimeters in diameter resulting in a gas flow of about 10 cc/hr. Total beam currents in low voltage set-ups run as high as a milliampere, of which about half is due to protons.

It is very difficult to compare the merits of the various kinds of sources which have been described. All of them are capable of producing ion currents of a milliampere with reasonable proton fractions in low voltage installations. In high voltage accelerators, however, the beam current is limited to a small fraction of this value by breakdown of the accelerating column. It cannot be emphasized too strongly, therefore, that an ion source is not to be judged simply upon the proton current which

it can deliver to a collector. The ions must emerge from the source with reasonably small transverse velocities if they are to be focused so as not to strike the accelerating electrodes. This restriction, as well as the need of a monoenergetic beam, argues against the use of a probe to extract the ions from the discharge. Moreover, it will be shown in Chapter V that if an analyzer is to be used to select ions of a certain energy from the beam, the exit hole of the source must be small if a reasonable fraction of the beam is to pass through the analyzer slits. Thus a high current density at the hole is a desirable feature. In addition, the operating life of the source, its efficiency (protons per H_2 molecule), and the fraction of the ions which are protons must be considered.

Development of a New High Frequency Ion Source

In order to become familiar with the performance of ion sources, a Zinn source was constructed similar to the one which was being used in the 1.4 Mev electrostatic accelerator in the Kellog Radiation Laboratory. According to the usual practice, it was first assembled with a probe just beyond the exit hole to "suck" the ions out of the discharge and start them down the accelerating column. A typical performance curve is shown in Fig. 9. In general, the focused beam current was divided

about evenly between the three types of ions. The highest proton current ever measured with this source was 7 μa.

It is significant that the unresolved current which could be focused through a $\frac{1}{4}$" hole was less than half the total beam current which was collected through a 2" aperture. This very considerable amount of stray ion current can be associated with the use of a probe. Presumably, those ions which manage to pass through the probe canal, but are not scattered, can be sharply focused; while those which are scattered in the canal without being neutralized acquire too much transverse velocity to be focused, and appear as stray ions. Although the probe may perform its function of extracting a large number of ions from the arc, only a small fraction of these contribute to the useful current, and as much appears as stray ion current.

The probe was eliminated and a new ion gun was constructed so that the ions diffusing through the exit hole would be accelerated and focused upon the target. Essentially the same focused ion currents were obtained with this arrangement, except that the stray ions were reduced to the point where the total current was only about 10% greater than that focused through the $\frac{1}{4}$" aperture.

It was felt that efforts to develop a better ion

source should be directed towards dissipating a large amount of power in a small volume. In this way, a high degree of dissociation into atomic hydrogen might be expected, resulting in high efficiency and an increased fraction of mass one ions. Such a performance has been reported with direct current discharges, but always with rapid deterioration of the cathode. A high frequency electrodeless discharge appeared to be well suited to the purpose, and offered the advantage of simplicity of construction.

The first radio frequency source (Fig. 10a) consisted of a quartz capillary, 1½ mm in diameter and 4 mm long inside, connected across the open end of a quarter-wave coaxial line fed by a 300 mc/sec oscillator having an available output power of 15 watts. Hydrogen flowed into one end of the capillary from the center conductor and passed out through an exit hole of 1/32" diameter at the other end. An electromagnet supplied an axial magnetic field which, it was hoped, would have a beneficial effect upon the discharge by limiting the transverse motions of the charged particles. Unfortunately, it proved impossible to strike an arc, presumably as a result of excessive recombination opportunities due to the large ratio of surface to volume of the chamber.

In the next attempt, the capillary was changed to a

quartz cylinder 8 mm in diameter and 12 mm long. (Fig. 10b) This time it was possible to strike the arc provided the magnetic field was applied. An 80 μa beam was obtained, containing 12% protons. The magnetic field was quite effective in increasing both the ion current and the proton fraction, as had been hoped. After a half-hour of operation, a deposit of metal of sufficient thickness to short out the discharge was sputtered upon the inside of the quartz cylinder.

In order to avoid sputtering from the metal surfaces at the ends of the cylinder, a third source, shown in Fig. 10c, was built in which the discharge chamber consisted of a barrel-shaped quartz bottle with a 1/32" hole in each lid for the flow of hydrogen and ions. A fuse-wire gasket at each end provided the vacuum seal. This source yielded an unresolved ion current of 45 μa containing 33% protons.

A number of other discharge chambers were tried, all having roughly the same volume as the last two just mentioned, but using different types of construction: aluminum ends, all metal chambers, etc. It was concluded from such tests that the presence of exposed metal in the discharge chamber greatly reduces the proton fraction in the beam. This result had been expected as it is well known that recombination coefficients for atomic hydrogen

are generally higher for metals than for insulators. This result is in agreement with the findings of the British investigators[16,17], who find it necessary to go to extreme measures to exclude metals from the arc plasma.

Using the barrel-shaped construction of Fig. 10c, further experiments were conducted to improve the performance. Water vapor, illuminating gas, and alcohol were added to the hydrogen in an effort to increase the proton fraction, but always with negative results. A new oscillator, capable of higher power and frequency (20 watts at 500 mc/sec), was constructed and increased yields resulted: 20, 17, and 13 μa for the mass one, two and three components respectively.

Continuing in this direction, a 70 watt, 450 mc/sec oscillator was built and the R. F. plumbing system was improved so that most of the available power could be delivered to the discharge chamber. The proton yield was quadrupled by this change, typical figures being 80, 40, and 10 μa for the three beam components.

The ion currents were still further increased by using a pyrex discharge chamber and enlarging the exit hole from .032" diameter to .042", and the hole in the first accelerating electrode from .08" to .12". Proton currents of over 300 μa were obtained following these

modifications.

A dozen different barrel-shaped discharge chambers have been used in an attempt to determine the proper construction. Some of the conclusions must be considered as preliminary, since a large number of variables are involved and many of these have not been fully investigated.

Effect of Changing Oscillator Frequency and Power

It seems reasonable to expect that the length of the discharge chamber should be made greater than the amplitudes of oscillation of the electrons due to the radio frequency field. This amplitude is proportional to the field strength divided by the square of the frequency. (See page 27) If the amplitude of oscillation is too large, a considerable fraction of the power input is lost by bombardment of the ends of the discharge chamber. The power which may be dissipated in the discharge for a given amplitude of oscillation increases very rapidly with frequency because the energy of each electron increases as the square of the frequency, and because the more intense discharge results in a larger number of electrons being present.

Under certain circumstances, it is observed that the ion yield increases very slowly with the available oscillator power above a certain power level. This saturation effect was first observed at 300 mc. Using a discharge

chamber .5" long and .33" in diameter, it was found that increasing the oscillator output beyond five or ten watts resulted in very little more ion current. Saturation was reached at about thirty watts at 450 mc/sec, using a chamber .27" in diameter and .4" long. This effect was not present when larger chambers were used at this same frequency.

Effect of Changing Diameter of Discharge Chamber

The magnetic field required to produce maximum ion current decreases as the diameter of the chamber is increased. With a diameter of .27", a field of about 2000 gauss is required; a .4" diameter chamber functions best at about 800 gauss. It will be seen that the ions in the discharge can hardly have energies as high as one electron volt, so their helical paths in the magnetic field have diameters small compared to that of the discharge chamber. This indicates that one function of the magnetic field is to bend the paths of the protons in the discharge enough to reduce the number of collisions which they make with the walls of the discharge chamber, thus reducing recombination.

Effect of Axial Magnetic Field

In the absence of a magnetic field, the discharge is rather faint, and a pale pinkish-blue in color. The field greatly intensifies the discharge and changes its

color to a bright red. This is to be contrasted to the cold watery-blue color of the D.C. discharge observed in the Zinn source. It is believed that the red color of the discharge is due to the atomic hydrogen ($H\alpha$) indicating a large degree of dissociation.

If the effect of the axial magnetic field were only to reduce the number of collisions with the walls of the chamber, the ion yield would be expected to increase monotonically with field strength. Such is not the case, however, as may be seen from a typical curve shown in Fig. 11. In general, there are numerous maxima and minima in the yield, with one or two main maxima near one or two thousand gauss. It is quite likely that this unexpected behavior is associated with a radial component of the magnetic field, as will be discussed in Chapter IV.

It is frequently observed that the discharge has a bright central core when a strong magnetic field is applied. The center conductor of the quarter-wave line, which applies the R. F. voltage to the discharge chamber, is made of iron so as to increase the magnetic field, and contains a hole through which the hydrogen flows. The central core appears to be most pronounced when this inlet hole is of large diameter, indicating that the core is due to an inhomogeneous magnetic field. Ion yields seem to be independent of the existence of this core.

Susceptance of the Discharge

A rough idea of the radio frequency susceptance of the discharge may be obtained by noting the shift in position of the tuning plunger required to tune the quarter-wave line to resonance after the discharge starts. If the susceptance were due only to free charges in the presence of the radio frequency field, the discharge should appear inductive, corresponding to a dielectric constant K less than unity as given by the equation[18]

$$K = 1 - 4\pi \frac{Ne^2}{m\omega^2} \qquad \text{(e.s.u.)}$$

where there are N charged particles of charge e and mass m per unit volume in the presence of the field of angular frequency ω.

It is observed that, in the absence of an axial magnetic field, the discharge appears to have an inductive susceptance of about .0002 mhos, corresponding to an electron density of 2×10^9 electrons per cc. At the same time, there are 10^6 times as many gas molecules present, and yet proton efficiencies of 10^{-3} protons per hydrogen molecule are measured. Since the net charge in the chamber must vanish, there must be one negative charge for each proton, and it follows that only about 0.1% of the negative particles in the discharge can be free electrons. It would thus appear that when the

magnetic field is removed, the discharge is sufficiently feeble that the electrons become attached to neutral particles and, therefore, do not contribute appreciably to the susceptance.

Under normal operating conditions, when the magnetic field is applied and the discharge is a bright red, a capacitive susceptance of about .001 mhos is observed. This effect was entirely unexpected and is probably due to a small radial component of the magnetic field, as will be indicated in Chapter IV.

Effect of Rate of Hydrogen Flow

The R. F. discharge may be maintained over a very wide range of hydrogen flow rates. At flows of less than 2 cc/hr, with a .04" exit hole, the discharge is very faint and is extinguished by application of the magnetic field. Between 2 and 15 cc/hr, the discharge is intensified by the field and the ion current is mostly due to molecular hydrogen. (See Fig. 12) Above 15 cc/hr, the discharge is much more intense and the ion beam consists largely of protons. The equipment was not able to handle hydrogen flows greater than about 70 cc/hr without sparking troubles.

General Observations

Cleanliness of the discharge chamber appears to be essential for proper operation of the source. It is

frequently observed that a newly assembled chamber will not function properly for an hour or two. The yield gradually increases by as much as a factor of two until normal output is attained.

The ion output appears to increase in proportion to the area of the exit hole, as might be expected. The diameter of this hole is limited by the gas flow which can be tolerated. In a high voltage accelerator, a rather small hole might be necessary in order to avoid breakdown of the column.

No evidence of deterioration of the ion source has been observed after more than ten hours of operation. A slight discoloration on the inside of the chamber is sometimes noted, but it appears not to be harmful.

It has been common practice to cool the discharge chamber with an air blast. This procedure may not be necessary, especially if a quartz chamber is used. The ion sources used in this investigation were built so as to be easily changed. In a more permanent installation it might be well to use a quartz discharge chamber enclosed in the vacuum envelope. Quartz appears to be slightly inferior to pyrex in regard to the ion currents which may be obtained, but it possesses much better mechanical properties.

IV. ANALYSIS OF THE RADIO FREQUENCY DISCHARGE

General Considerations

An understanding of the discharge mechanism would be of considerable value in the further development of the ion source. While some aspects of the problem are not fully understood, it is, nevertheless, possible to establish the general nature of the phenomenon.

Under normal operating conditions where maximum proton current is obtained, the source requires a hydrogen flow of roughly 40 cc/hr for a .040" diameter exit hole. In the absence of a discharge, a pressure of .1 mm Hg in the chamber is calculated from the Knudsen equations of gas flow. It will be shown that the discharge heats the gas up to a temperature of no more than a few thousand degrees Centigrade so that the density is decreased by a factor of five or less. This indicates a mean free path of somewhat less than a centimeter for hydrogen and several centimeters for the electrons. It follows that collisions with the walls are as frequent as collisions between particles in the discharge.

It is easily seen that a particle of specific charge e/m in an alternating field of strength E and angular frequency ω executes an oscillation of half-amplitude

$$x = \frac{eE}{m\omega^2}$$

and attains a maximum energy

$$W = \frac{Ex}{2} = \frac{eE^2}{2m\omega^2}$$

The field strengths involved are estimated to be of the order of 300 volts/cm. With a 450 mc/sec excitation frequency, the electrons have half-amplitudes of .7 mm and energies of 10 electron volts. Protons and other heavy ions are hardly affected by the field; they move less than a micron and receive about .005 electron volts from the field. It would thus appear that energy is contributed to the discharge through the agency of the electrons which heat up the rest of the gas and cause dissociation and ionization by their relatively high energies.

There appears to be no mechanism whereby the electrons can deliver more than a small fraction of their average energy to the heavy particles of the discharge. The number of electrons present in the discharge is fairly well known from the susceptance measurements. From this data, it can be calculated that the heavy particles collide with the walls of the chamber hundreds of times as often as they do with electrons, so they receive very little energy by direct collisions with electrons.

It is quite likely that electrons are collected on

the ends of the discharge chamber, thereby producing static fields which attract the less mobile heavy ions of the discharge. The fields may be strong enough to give the ions several electron volts of energy which they could pass on to other particles by collisions. Since most of the heavy particles are not ionized, their average energy must be considerably less than one electron volt.

It is observed that the discharge exhibits a deep red color indicating a high degree of dissociation into atomic hydrogen. The high proton yields obtained further indicate that most of the gas exists in the atomic state. This might seem to be surprising, since collisions with the walls of the chamber are so frequent. However, measurements by W. V. Smith[19] show that with pyrex vessels, only one wall collision in 10^4 or 10^5 results in recombination. Since a molecule encounters an electron once in every few hundred wall collisions, the high degree of dissociation may be accounted for if a reasonable fraction of the electrons are sufficiently energetic to dissociate the hydrogen. This is evidently the case, since the binding energy of the hydrogen molecule is only 4.4 electron volts and the electrons were seen to oscillate with more than twice this energy. Smith's measurements also showed that recombination is

ten times more frequent on quartz than on pyrex, and that nearly every collision with platinum results in recombination. This confirms the observation that pyrex discharge chambers were somewhat superior to quartz, and that metals were definitely to be avoided.

Motion of Charged Particles in a Magnetic Field

It is of interest to consider the motions of charged particles acted upon by an alternating force in the presence of a magnetic field. The mean free paths of the particles in the R. F. ion source discharge are long enough that a large number of oscillations are performed between collisions, and, therefore, it is sufficient to consider the motion of a single particle. Four effects are observed which apparently cannot be accounted for by a uniform axial magnetic field. At low rates of gas flow, the discharge is completely extinguished by a small magnetic field. At higher rates of flow, the discharge is enhanced by a moderate field, but both the brightness of the discharge and its ion yield are found to decrease again as the field is increased beyond about 2000 gauss, as shown by Fig. 11. The third characteristic is the bright central column observed in the discharge under certain conditions. Finally, it is found that the susceptance of the discharge, which is inductive in the absence of a magnetic field, becomes capacitive when the magnetic

field is applied.

The following discussion considers the motion of a charged particle in the presence of an axially symmetric magnetic field having a small radial component. The analysis indicates that the radial component probably accounts for the above characteristics, but does not yield quantitative results.

Consider a particle having specific charge e/m in the presence of an alternating electric field of strength E directed along the z-axis (axis of symmetry) and having an angular frequency ω. Let the axial component of the magnetic field be $B_z = B_0 (1+\alpha z)$ where α is a small quantity indicating the non-uniformity of the field. Since the divergence of the field vanishes, there must exist a radial component $B_r = -\frac{1}{2}B_0 \alpha r$. We shall investigate the nature of small oscillations about a point in the $z = 0$ plane at a distance r_0 from the axis. At that point we take a set of rectangular coordinates with the x-axis in the radial direction and the y-axis in the azimuthal direction. The magnetic field has components in this system given approximately by

$$B_x = -\frac{\alpha}{2} B_0 (r_0 + x)$$

$$B_y = -\frac{\alpha}{2} B_0 y$$

$$B_z = B_0 (1+\alpha z)$$

Using a dot to indicate a time derivative, the equations of motion are given in Gaussian units by

$$m\ddot{x} = \frac{e}{c}\left[B_0 \dot{y}(1+\alpha z) + \frac{\alpha}{2} B_0 \dot{z} y\right]$$

$$m\ddot{y} = \frac{e}{c}\left[-\frac{\alpha}{2} B_0 \dot{z}(r_0+x) - B_0 \dot{x}(1+\alpha z)\right]$$

$$m\ddot{z} = \frac{e}{c}\left[-\frac{\alpha}{2} B_0 \dot{x} y + \frac{\alpha}{2} B_0 \dot{y}(r_0+x)\right] + Ee \cos \omega t$$

It is convenient to introduce the cyclotron frequency $\omega_c = eB_0/mc$, and the amplitude of oscillation $A = eE/m\omega^2$ which the particle would have in the absence of the radial field. These equations may be solved using a perturbation method by expanding in powers of the small quantity α:

$$x = x_0 + \alpha x_1 + \alpha^2 x_2 + \cdots$$

$$y = y_0 + \alpha y_1 + \alpha^2 y_2 + \cdots$$

$$z = z_0 + \alpha z_1 + \alpha^2 z_2 + \cdots$$

Successive approximations to the motion of the particle are obtained in the usual fashion by substituting these expressions into the equations of motion, and collecting terms involving the same powers of α. We obtain:

Zero-order approximation

$$\ddot{x}_0 = \omega_c \dot{y}_0$$

$$\ddot{y}_0 = -\omega_c \dot{x}_0$$

$$\ddot{z}_0 = A\omega^2 \cos \omega t$$

First-order approximation

$$\ddot{x}_1 = \omega_c \dot{y}_1 + \omega_c \dot{y}_0 z_0 + \frac{\omega_c}{2} y_0 \dot{z}_0$$

$$\ddot{y}_1 = -\omega_c \dot{x}_1 - \frac{\omega_c}{2} r_0 \dot{z}_0 - \frac{\omega_c}{2} x_0 \dot{z}_0 - \omega_c \dot{x}_0 z_0$$

$$\ddot{z}_1 = -\frac{\omega_c}{2} \dot{x}_0 y_0 + \frac{\omega_c}{2} r_0 \dot{y}_0 + \frac{\omega_c}{2} x_0 \dot{y}_0$$

Second-order approximation

$$\ddot{x}_2 = \omega_c \dot{y}_2 + \omega_c \dot{y}_1 z_0 + \omega_c \dot{y}_0 z_1 + \frac{\omega_c}{2} y_0 \dot{z}_1 + \frac{\omega_c}{2} y_1 \dot{z}_0$$

$$\ddot{y}_2 = -\omega_c \dot{x}_2 - \frac{\omega_c}{2} r_0 \dot{z}_1 - \frac{\omega_c}{2} x_0 \dot{z}_1 - \frac{\omega_c}{2} x_1 \dot{z}_0 - \omega_c \dot{x}_0 z_1 - \omega_c \dot{x}_1 z_0$$

$$\ddot{z}_2 = -\frac{\omega_c}{2} \dot{x}_0 y_1 - \frac{\omega_c}{2} \dot{x}_1 y_0 + \frac{\omega_c}{2} r_0 \dot{y}_1 + \frac{\omega_c}{2} x_0 \dot{y}_1 + \frac{\omega_c}{2} x_1 \dot{y}_0$$

The zero-order solution consists of axial oscillations of amplitude A superimposed upon circular motions in the x-y plane having arbitrary radius R and the cyclotron frequency ω_c:

$$x_o = R \cos(\omega_c t + \delta)$$

$$y_o = -R \sin(\omega_c t + \delta)$$

$$z_o = -A \cos \omega t = -\frac{eE}{m\omega^2} \cos \omega t$$

A term corresponding to a constant velocity in the z-direction has been dropped since it would not appear to be essential to the discussion.

The electrons in the discharge are likely to have transverse velocities comparable to their oscillation velocities, so $\omega_c R$ is roughly equal to ωA. In the usual operating field of 1500 gauss, the cyclotron frequency is 4200 mc/sec, or ten times the applied frequency, so the electrons execute helix-like orbits having diameters one-tenth the length of the helix.

The velocities of oscillation of protons in the discharge are considerably less than their thermal velocities, and the applied frequency is 200 times their cyclotron frequency. The corresponding orbits are, therefore, almost unaffected by the R. F. field, and it appears that the magnetic field affects the heavy ions only inasmuch as it reduces the number of collisions which they make with the sides of the discharge chamber. The subsequent discussion, therefore, will be restricted to the orbits of the electrons in the discharge.

The first-order solutions are obtained in a straightforward manner. The axial motion consists of an oscillation at cyclotron frequency and a secular term representing a constant acceleration in the direction of weaker magnetic field intensity.

$$z_1 = -\frac{\omega_c^2 R^2 t^2}{4} + \frac{R r_0}{2}\cos(\omega_c t + \delta)$$

This acceleration term may contain the explanation for the fact that the magnetic field will extinguish the discharge at low rates of hydrogen flow. At higher pressures, charges may build up within the discharge chamber in such a way as to neutralize this term.

The transverse motions are more involved but turn out to be of the form

$$x_1 = \frac{r_0 A}{2}\frac{\omega_c^2}{\omega_c^2 - \omega^2}\cos\omega t + \frac{RA}{2}\frac{(\text{Terms in } \omega \text{ and } \omega_c)}{(\omega_c^2-\omega^2)(4\omega_c^2-\omega^2)}\cos(\omega_c t+\delta_1)\cos(\omega t+\delta_2)$$

It is evident that a resonance effect takes place when $\omega = \omega_c$ even in the absence of transverse velocities. The degree of non-uniformity of the field does not affect the frequency of this resonance, although the effect would be absent in a uniform magnetic field. The resonance simply becomes more pronounced as the non-uniformity is increased.

The resonance phenomenon provides an explanation for the change in sign of the susceptance of the discharge as

the magnetic field is increased. The effect is analogous to dispersion in dielectrics where the dielectric constant is first greater than unity and then less as the frequency is increased through a resonance region.

The second-order solutions show a resonance at half the cyclotron frequency, and an azimuthal precession linear in the time, which do not depend upon the presence of a zero-order transverse velocity. Higher order approximations might be expected to show further resonances at multiples or sub-multiples of the cyclotron frequency, thereby affording a possible explanation for the complicated nature of the yield as a function of the magnetic field strength. The secular terms which eject the electrons from the discharge probably account for the decrease in yield as the magnetic field is increased beyond the resonance region.

In the region of the gas inlet hole in the iron center conductor of the R. F. coaxial line, the magnetic field is quite inhomogeneous. With a large inlet hole, this inhomogenuity extends into the discharge chamber an appreciable distance, and may possibly account for the bright central core sometimes observed in the discharge.

The foregoing analysis indicates that some of the characteristics of the discharge may be accounted for by the presence of a small radial magnetic field component.

It is quite likely that the performance of the ion source might be considerably improved by a proper modification of the magnetic field. The field of the ion source described in this paper has been measured and was found to be about 25% stronger at the inlet end of the discharge chamber, but no systematic experiments have been conducted as yet to determine the effect of varying the inhomogenuity of this field.

V. ION GUN DESIGN

General Discussion

It has been general practice in the past to design the initial accelerating electrode system largely by trial and error. The optical properties of numerous electrostatic lenses have been worked out and, using this knowledge, it is possible to design ion guns whose operation is known with reasonable accuracy.

The ion gun should be constructed so as to satisfy, as well as possible, the following conditions:

a) The use of a probe to suck the ions out of the discharge is to be avoided, as it is a source of stray ions, and because it introduces an energy spread into the beam.

b) The electrodes should be designed, where possible, so that they represent lenses whose focal properties are known.

c) The focal length of the composite ion gun should be chosen according to the conditions to be met by the resulting beam. A short focus ion gun system will produce a large image of the exit hole formed by nearly parallel rays. Conversely, a lower magnification results in a sharp spot formed by more sharply convergent rays. This factor is of importance if the beam is to be sent through an analyzing system

to remove ions whose energy differs appreciably from the desired value.

d) If differential pumping is to be used to reduce the gas pressure in the column, the first accelerating electrode should have an opening only slightly larger than the beam diameter, located a small fraction of a mean free path from the exit hole. A pumping speed of 10 liter/sec for hydrogen (2 liter/sec for air) will handle a gas flow of 50 cc/hr at a pressure of 10^{-3} mm Hg, corresponding to a mean free path of 12 cm. This first accelerating gap should be made short to reduce the pumping speed requirements.

e) The first electrode should also be the aperture stop of the lens system so that it intercepts virtually all of the stray ions which would otherwise be collected by the electrodes of the accelerating column.

f) Because of the rather large current collected by the first electrode, its voltage must be controlled by a variable power supply. For practical reasons, this voltage should not exceed about 20 kv.

Optics of Electrostatic Lens Systems

In the absence of space-charge effects, a very close analogy may be drawn between light optics and charged particle optics. A summary of the essential features of electrostatic lens systems will follow; the underlying

theory may be found in Zworykin's book[5] on electron optics.

The trajectories of charged particles in an electrostatic field are the same as those of light rays in a medium whose refractive index varies as the square root of the electrostatic potential ϕ, where ϕ vanishes at a point where the particles are at rest. The formulae of geometrical optics may be used simply by replacing the index of refraction by $\phi^{\frac{1}{2}}$. Thus, the magnification m of a lens system is

$$m = -\frac{f_o d_i}{f_i d_o} = -\frac{f_o}{d_o - f_o}$$

where f_0 and f_1 are the object and image side focal lengths, and d_0 and d_1 are the distances of object and image from the principal planes.

It is to be understood that the lens equations apply to field-free object and image spaces at potentials ϕ_0 and ϕ_1 respectively. In the event that one side of the lens is not a constant potential region, the characteristics of the lens are determined in terms of an imaginary field-free space having the potential of a convenient reference point.

The focal lengths of a lens are related to the potentials by the expression

$$\frac{f_o}{f_i} = \left(\frac{\phi_o}{\phi_i}\right)^{1/2}$$

The angles of divergence Θ_0 and Θ_1 of the limiting rays which leave the object and which form the image, satisfy the equation

$$\theta_i = \frac{\theta_0}{m}\left(\frac{\phi_0}{\phi_i}\right)^{1/2} \qquad 41\text{-}1$$

Neglecting relativistic effects, the focal properties of an electrostatic lens are determined by the geometry and potential ratios of the conductors, and are independent of the absolute values of these potentials and of the specific charge of the particles. Accordingly, the different kinds of particles in the ion beam cannot be separated by electrostatic means, nor by space-charge effects.

A further characteristic of electrostatic lenses arises from the fact that the electric fields satisfy Laplace's equation. If a lens is such that the rays cross the axis of symmetry no more than once, and if real field-free object and image spaces exist, then the lens always exerts a positive focusing action. Negative lenses can only arise as combinations of such simple lenses, or when an accelerating field exists on one or both sides of the lens.

The Two-Cylinder Accelerating Lens

Perhaps the most commonly used accelerating lens consists of two cylinders at potentials ϕ_0 and ϕ_1 spaced

a small distance apart. The focal properties of such a lens are shown in Fig. 13 as given by Goddard[4]. It is to be noted that the principal planes are crossed and are both on the object side.

The Single-Aperture Lens

Two uniform accelerating fields of different strengths, separated by a conducting sheet with a hole of diameter D in the center, constitute an example of a lens not bounded by field-free object and image spaces. The presence of the hole causes the rays to be deflected in passing through, so that the parabolic trajectories do not join smoothly. If imaginary field-free spaces having the potential ϕ_s of the sheet are assumed, the focal length of the aperture lens is given by

$$f_o = f_i = \frac{4\phi_s}{\phi_i' - \phi_o'} + \frac{2D}{\pi} \qquad 42\text{-}1$$

where the prime indicates a derivative along the axis of symmetry. This formula is fairly accurate if the radius of the hole is less than the ratio of ϕ_s to ϕ_o' or ϕ_i'.

The Cathode Lens

The name is a carry-over from electron optics and applies to the electrodes used to accelerate the particles from a surface which they leave with nearly zero velocity. A commonly used cathode lens consists of a uniform accelerating field between the plane cathode or anode surface,

and a screen a distance d away having a small hole to admit the beam. Referred to a field-free space on the image side of the screen, the object appears to be 2/3 its actual size and to be a distance 4d/3 behind the screen (d/3 behind the cathode or anode surface).

Space-Charge Effects

The mutual repulsion between the particles of the beam must sometimes be taken into account in calculating the performance of the accelerating system. In electron-optical systems where high resolution is required, only a slight amount of space-charge spreading can be tolerated. The effects are not so serious in electrostatic accelerators since it is only required that the image of the exit hole be not blurred out to more than about twice its area.

It will be shown that a source emitting a constant current density in a radial direction within a cone of half-angle θ about the beam axis, and with no current outside the cone, may be imaged to a sharp disc of uniform intensity. The size of this disc may be calculated and yields a lower limit to the diameter of the beam which may be obtained at the target.

The equations of motion of a beam of charged particles have been worked out by Thompson and Headrick[21]. They consider an axially symmetric beam of particles

having specific charge e/m all directed along the z-axis with the same velocity v in an otherwise field-free space. It is assumed that the radial velocity is much less than the axial velocity v, and that particles which initially are closer to the axis than others remain so as they move along. Under all practical circumstances connected with electrostatic accelerator beams, the charge distribution within a cylinder of radius r which carries a current i may be considered to be continuous, so that a particle on the surface of such a cylinder experiences a radial force

$$m\frac{d^2r}{dt^2} = mv^2\frac{d^2r}{dz^2} = \frac{2ei}{vr} \qquad 44\text{-}1$$

Writing the velocity v in terms of the accelerating potential ϕ and integrating twice gives

$$\frac{dr}{dz} = \left(\frac{2mi^2}{e\phi^3}\right)^{1/4}\left(\log\frac{r}{r_o}\right)^{1/2} \qquad 44\text{-}2$$

$$\left(\frac{mi^2}{8e\phi^3}\right)^{1/4}\frac{z}{r_o} = \int_0^{\left(\log\frac{r}{r_o}\right)^{1/2}} e^{x^2}\,dx \qquad 44\text{-}3$$

Initial conditions have been chosen such that at z = 0, all the particles are moving exactly parallel to the z-axis and the cylinder which contains the current i has a radius r_o.

The results of Thompson and Headrick may be extended and put into convenient form for use in connection with ion beams. Since the contribution of an ion to the space-charge field is proportional to the square root of its mass, it is appropriate to define an equivalent proton current $I = i_1 + \sqrt{2}i_2 + \sqrt{3}i_3$. A pure proton beam of current I experiences the same spreading as the actual beam does which consists of the three mass components.

The last equation, expressed in terms of the equivalent proton current I in μa and the potential in Mv, becomes

$$\frac{I^{1/2}}{\phi^{3/4}} \frac{z}{r_0} = 5.53 \times 10^{4} \int_0^{(\log \frac{r}{r_0})^{1/2}} e^{x^2} dx$$

This equation is plotted in Fig. 14, and illustrates the manner in which the beam diverges due to its own space-charge repulsion.

It is seen by inspection of equations 44-2 and 44-3 that if the current density in the beam is uniform (I proportional to r^2), at z = 0 the density remains uniform as the particles move along, and the radial velocity is proportional to the radius r. Such a beam can, therefore, be focused by lenses and any cross-section will continue to have a uniform current density.

A beam of initial radius r_i may be focused by a lens so as to have a minimum radius r_m at a given distance z from the lens, the value of r_m being determined by the space-charge repulsion. The curve of r_m as a function of z is the envelope of the family of beam trajectories of varying angle of convergence, and is shown in Figs. 15 and 16.

It may easily be seen from Fig. 14 that the maximum equivalent proton current which can be sent through two irises of diameter d separated by a distance l as limited by space-charge depends only upon the beam energy ϕ and the ratio of d to l, and is given by the formula

$$I = 9.0 \times 10^{6} \frac{d^2}{l^2} \phi^{3/2}$$

Thus at one Mev, a maximum of 225 μa of proton current can be sent through two holes 1 mm in diameter and 2 m apart.

Pierce Gun

Space-charge repulsion is evidently most effective in the first accelerating sections where the beam has low velocity, and particularly in the cathode lens. A method of accelerating a beam of charged particles from rest in such a way as to neutralize their mutual repulsion was worked out by J. R. Pierce[22]. The accelerating electrodes are shaped so as to produce an axial potential

distribution given by

$$\phi = \left[\frac{81\pi^2 j^2 m}{2e}\right]^{1/3} z^{4/3}$$

where j is the equivalent proton current density. Expressing the potential in volts, j in amps per cm^2, and z in cm, gives

$$\phi = 7.0 \times 10^{4} j^{2/3} z^{4/3}$$

It is to be expected that use of the Pierce Gun technique in the initial accelerating gap produces essentially the same beam characteristics as would be obtained by using a uniform accelerating field in the absence of space-charge repulsion.

The accelerating gap shown in Fig. 3 consists of a Pierce Gun, somewhat modified in the neighborhood of the exit hole. The hole in the accelerating electrode has the effect of a negative lens as given by equation 42-1. This lens is 4/3 as strong as that of the corresponding electrode of the "cathode lens" described earlier, so the characteristics of the Pierce Gun are slightly different from those of the uniform field cathode lens. This difference is quite small, however, and will not be taken into account. The Pierce Gun will be regarded as a means of overcoming the space-charge effects

in the usual cathode lens without otherwise changing its characteristics.

Effect of the Exit Hole

The nature of the beam as it enters the accelerating field of the cathode lens is complicated by the fact that ions are not emitted from a plane conducting surface as is the case with electrons, but enter the field through a small hole in the electrode. The fringing field of the accelerating potential extends into this hole, and its transverse component imparts a lateral velocity to the emerging ions.

Within the discharge, the arc plasma consists of a nearly equal number of positive and negative particles. The electrons have approximately ten electron volts of random energy, while the heavy particles possess energies of a small fraction of an electron volt. The fringing field of the exit hole repels the electrons, leaving an excess of positive ions. If a Pierce Gun is used as the first accelerating potential, its field is adjusted so that space-charge limited flow exists at the exit hole. In this case, the fringing field terminates upon the excess positive ions instead of on the inside of the exit hole. The transverse component of the fringing field is thereby reduced, so the emerging ions possess only a small transverse velocity.

This transverse velocity may be estimated from a measurement of the fraction of the ion current collected by the Pierce Gun accelerating electrode. To a first approximation, the ions move as though they were in a uniform field and, therefore, travel in a parabolic path. Starting with an initial transverse energy E_t, they arrive at the accelerating electrode a distance d away with energy E, and at a distance r from the axis.

$$\frac{r}{d} = 2\sqrt{\frac{E_t}{E}}$$

The ions passing through a .080" diameter hole in the accelerating electrode which is at a potential of 7000 volts, and .4" from the exit hole, can have an initial transverse energy of only 18 electron volts. Since about half the current passes through such a hole, this figure is roughly equal to the average transverse energy of the ions.

Choice of Ion Gun Electrode System

It would seem reasonable to use a Pierce Gun as a cathode lens, since it is capable of producing a well collimated beam whose characteristics are fairly well known. Before entering the accelerating column, the beam must be made to pass through a lens which will cause the ions to converge upon the target. Since the cathode lens changes the apparent size and position of the object only

slightly, and since the accelerating column is generally constructed so as to exert very little focusing action, this lens is largely responsible for the properties of the resulting image. Furthermore, the object side focal length of this lens is nearly the same as the object side focal length of the entire accelerating system, since the accelerating column acts like a medium whose index of refraction varies in the axial direction only. On the basis of this simplified viewpoint, it is a simple matter to choose the focal length necessary to give an image of the desired magnification.

The Pierce Gun produces an ion beam in a field-free space; the accelerating column consists of a nearly uniform field. Accordingly, the main focusing lens must have a field-free object space and an image space which has the same potential gradient as does the accelerating column. The single-aperture lens described on page 42 has this property. In this application, the object-side potential gradient is zero so the object space is real and its focal length is simply

$$f_o = \frac{4\phi_o}{\phi_i'} + \frac{2D}{\pi}$$

A two-cylinder lens might have been used for the main focusing lens, but in that case the discontinuity between its field-free image space and the accelerating field of the column would have produced a second fairly strong lens which would complicate the problems of construction and analysis. This arrangement is the one actually used in the ion gun shown in Fig. 3. The first focusing lens was built with a rather short focal length so that a considerably enlarged image of the exit hole was produced upon the target. When this gap was shorted out, the second focusing lens, being a single-aperture lens of a long focal length, produced a pin-point image upon the target.

Choice of Focal Length of the Accelerating Column

For many purposes, it is sufficient to produce an image no larger than about a millimeter diameter upon the target. In this case, a magnification of unity or less is all that is required of the lens system. Equation 41-1 shows, however, that as the magnification is reduced, the angle of convergence of the rays which form the image increases. If this angle of convergence is important, as is the case if the beam is to be sent through the slit system of an energy analyzer, then it is necessary to make a compromise between the size of the image and the angle of convergence which may be tolerated.

Consider, for example, an ion source using a probe to extract the ions from the discharge. If the probe has a 1 mm diameter canal 5 mm long, then the ions which pass through without being scattered are confined to lie within a cone of .2 radian half-angle. Ions which are scattered would not be expected to focus properly and need not be considered. If the magnification is unity with 1 kv probe voltage, and 1 Mv accelerating voltage, a 1 mm spot would be obtained with a half-angle of convergence of .006 radians, as calculated from equation 41-1. Most of this current would be lost in going through an analyzer having 2 mm slits 2 m apart.

As another example, the convergence of the beam coming from a diffusion type ion gun, as shown in Fig. 3, will be computed. The ions which manage to pass through the opening in the first accelerating electrode were seen to start with a transverse velocity corresponding to about 20 electron volts. They are restricted by the geometry near the exit hole to lie within a cone having a half-angle of about one radian, so using 1 Mv accelerating potential and unity magnification as before, the half-angle of convergence of the resulting beam turns out to be about .005 radians. A magnification of two would permit a considerably larger fraction of the beam current to pass through such an analyzer.

A magnification of two is obtained when the image distance is three focal lengths from the corresponding unit plane. The unit planes are located close to the aperture lens and the image distance is nearly equal to the distance between ion source and target. At 1 Mv accelerating voltage, and using a 7 kv Pierce Gun potential, the ratio of image to object focal length is 12. Thus, with a distance of 20 feet between source and target, a 7" object side focal length is needed for the accelerating system exclusive of the Pierce Gun. The aperture lens, therefore, must have a focal length of over 7", corresponding to an aperture diameter of about 8". Such an aperture is inconveniently large, so it is advisable to increase the effective diameter of the lens by lowering the voltage applied to the first electrode of the accelerating column. This smooths out the potential gradients and gives the effect of a larger diameter aperture lens.

VI. FOCAL PROPERTIES OF ACCELERATING COLUMNS

Introduction

It is convenient to regard the accelerating field near the axis of the column as being that of a uniform field modified by the presence of the accelerating electrodes. An initially diverging beam cannot be made convergent by a uniform electric field, so such a field will have no focusing properties. It is analogous to a medium whose refractive index varies in one direction only. A column whose electrodes consist of thin annular discs will, therefore, have an infinite focal length, since the discs do not disturb the uniform field. Electrodes which have a finite extension along the axis will modify the field and thus produce a focusing effect.

The electrodes of an accelerating column are frequently made in rather complicated shapes (as in Fig. 3, for example) in order to shield the insulators from the beam without decreasing the electrode spacing to the point where field emission would cause breakdown. In such cases, the spacing is generally small compared with the length of a section, and the diameter of an electrode does not differ more than perhaps 25% from its average diameter; so the field along the axis of the column does not differ significantly from that of an idealized column whose electrodes are closely spaced sections of cylinders having the

average diameter of the electrodes of the actual column. The details of the construction of the electrodes give rise to high order harmonics of the potential which damp out rapidly as the axis is approached. The focal properties of most accelerating columns may, therefore, be determined with reasonable accuracy from a study of the trajectories of ions moving near the axis of a series of closely spaced cylinders whose potentials increase linearly from one cylinder to the next.

A somewhat similar problem arises in connection with linear accelerators where the situation is made more complicated by the need for phase stability in order that the ions may be properly accelerated at each gap by the radio frequency driving voltage. Analyses of linear accelerator focusing such as that of Hansen and Webster[23] are not applicable to the problem of focusing in constant voltage accelerators, however, because of the prominent role played by the phase stability requirement. Moreover, the accelerating cylinders are generally considered to be long compared with their diameter, and the lengths increase with the ion energy.

The problem of focusing in constant voltage accelerators may easily be solved in two cases. If the ratio of the radius a to the length b of a cylinder is small, the field very nearly vanishes in the center of a cylinder,

and the focal properties of each gap are essentially those of the two-cylinder electrostatic lens whose characteristics are well known[4]. The properties of a succession of such lenses are obtained by successive application of the usual lens equations of optics. This method of analysis may be used if the ratio of radius to length is less than $\frac{1}{4}$ since in this case the field strength in the center is less than 4% of its maximum value.

If, on the other hand, the ratio of radius to length is more than $\frac{1}{2}$, the axial field consists essentially of a sinusoidal fluctuation superimposed upon the uniform field. The second harmonic axial variation is 6% of the fundamental at a ratio of $\frac{1}{2}$ and decreases very rapidly as the ratio increases. The optical properties of short cylinder columns will be worked out in later sections.

It is a familiar fact that the focal power of a two-cylinder electrostatic lens decreases rapidly as the voltage ratio of the cylinders approaches unity. For this reason, the initial accelerating gaps, where the voltage increments are comparable to the voltage of the beam, contribute most strongly to the focal power of the column. Nevertheless, in long columns the small contributions from the high energy electrodes are appreciable and will be taken into account.

In short cylinder accelerating columns, a transition

region must exist between the nearly uniform accelerating field and the field-free region which generally exists between the ion source and the column itself. Such a transition constitutes a strong lens and must be taken into account. A discussion of this lens has been given in Chapter V, page 50. It will, therefore, be assumed that the accelerating column consists of an infinite array of coaxial cylinders, and our problem is to determine the focal properties of any n sections of the column in which the beam has a positive energy.

Focal Properties of a Single Section

We shall consider an infinite series of cylinders of radius a and length b separated by a negligible gap, and whose axes lie along the z-axis. The n-th cylinder is centered at $z = (n-1)b$ and has a potential $V_n = V_o\left[1+(n-1)v\right]$ where v is the ratio of the gap voltage to the voltage of the cylinder at the origin. The potential at which the beam has no velocity will be taken to be zero.

The motion of a charged particle which is moving nearly parallel to the axis of symmetry of an electrostatic field is governed by the paraxial ray equation

$$\frac{d^2r}{dz^2} = -\frac{1}{2\phi}\frac{d\phi}{dz}\frac{dr}{dz} - \frac{1}{4\phi}\frac{d^2\phi}{dz^2}r$$

where ϕ is the potential distribution along the axis of

symmetry (z-axis) and r is the distance of the particle from the axis.

It is easily seen that the axial potential distribution is given by

$$\phi = V_o \left\{ 1 + v\frac{z}{b} + \sum_{m=1}^{\infty} \frac{v}{\pi} \frac{(-1)^m}{m} \frac{I_o(0)}{I_o\left(\frac{2\pi m a}{b}\right)} \sin \frac{2\pi m z}{b} \right\}$$

where I_o is the zero-order Bessel Function of imaginary argument which is finite on the axis. The ratio of $I_o(2\pi ma/b)$ to $I_o(4\pi ma/b)$ is .06 for $a/b = \frac{1}{2}$ and decreases rapidly as a/b increases, so all but the first term of the series may be dropped without serious error. Writing $\alpha = \frac{1}{2}I_o(0)/I_o(2\pi a/b)$, the axial potential is given approximately by

$$\phi = V_o \left\{ 1 + v\frac{z}{b} - \frac{2}{\pi} v\alpha \sin \frac{2\pi z}{b} \right\}$$

The sinusoidal term is small and may be regarded as a perturbation. We write

$$\phi = \phi_u + \phi_p$$

$$r = r_u + r_p$$

where the subscript p indicates a small perturbation term. The unperturbed potential represents the uniform field in which the particle follows a parabolic trajectory given by r_u.

$$\phi_u = V_o\left\{1 + \nu\frac{z}{b}\right\} \qquad 59\text{-}1$$

$$\phi_p = -\frac{2}{\pi} V_o \nu \alpha \sin\frac{2\pi z}{b} \qquad 59\text{-}2$$

$$r_u = r_o + 2 r_o' b\nu\left[\sqrt{1+\nu\frac{z}{b}} - 1\right] \qquad 59\text{-}3$$

r_o and r_o' give the position and slope respectively of the trajectory at the center of the first lens (at z = 0). Substituting these quantities into the paraxial equation and dropping all but the zero-order and first-order terms, we find that r_p is determined to a first approximation by

$$r_p'' = -\frac{\phi_u'}{2\phi_u} r_p' - \frac{\phi_p'}{2\phi_u} r_u' + \frac{\phi_u'\phi_p}{2\phi_u^2} r_u' - \frac{\phi_p''}{4\phi_u} r_u + \frac{\phi_u''\phi_p}{4\phi_u^2} r_u - \frac{\phi_u''}{4\phi_u} r_p$$

where the prime signifies differentiation with respect to z. To find the motion at the center of the second cylinder, we integrate twice and obtain (since $\phi_u'' = 0$)

$$r_{p1}' = \frac{1}{2\sqrt{\phi_u}}\int_o^b \left\{\left[\frac{\phi_u'\phi_p}{\phi_u} - \phi_p'\right] r_u' - \frac{1}{2}\phi_p'' r_u\right\}\frac{dz}{\sqrt{\phi_u}}$$

$$r_{p1} = \int_o^b \frac{dz}{2\sqrt{\phi_u}} \int_o^z \left\{\left[\frac{\phi_u'\phi_p}{\phi_u} - \phi_p'\right] r_u' - \frac{1}{2}\phi_p'' r_u\right\}\frac{d\zeta}{\sqrt{\phi_u}}$$

where r_{p1} and r_{p1}' are the position and slope at the center of the second cylinder. In the integration of these equations, terms of the form

$$\int_o^z \frac{\sin\left(\frac{2\pi z}{b}\right)}{\cos\left(\frac{2\pi z}{b}\right)} \frac{}{\left(1+\nu\frac{z}{b}\right)^{n+\frac{1}{2}}}\, dz$$

are encountered. A succession of integrations by parts yields rapidly convergent series in powers of v. Using these series, we obtain

$$r_{p1}' = 2\alpha\left(r_o' - \frac{v}{2b}r_o\right)\left\{\left[\frac{1}{\sqrt{1+v}} - \frac{1}{1+v}\right] - \frac{3v^2}{16\pi^3}\left[\frac{1}{\sqrt{1+v}} - \frac{1}{(1+v)^3}\right] + \cdots\right\}$$

60-1

$$r_{p1} = 2\alpha r_o\left\{\left(1-\sqrt{1+v}\right)\left(1 - \frac{3v^2}{16\pi^2} + \cdots\right) + \frac{3v^2}{16\pi^2}\left(1 - \frac{1}{(1+v)^2}\right) + \cdots\right\}$$

$$- \frac{3}{4\pi^2}\alpha b v r_o'\left\{\left(\sqrt{1+v} - 1\right)\left(1 + \frac{1}{(1+v)^2} - \frac{35v^2}{16\pi^2}\right) - \frac{35v^2}{16\pi^2}\left(1 - \frac{1}{(1+v)^4}\right)\right.$$

$$\left. + \frac{15v^2}{16\pi^2}\left(1 - \frac{1}{(1+v)^{7/2}}\right) + \cdots\right\}$$

60-2

Terms have been neglected which contribute only a few percent even when v = 1 and which decrease rapidly with v. When v is small, it is convenient to expand these expressions directly in powers of v. We find

$$r_{p1}' = \alpha v\left(r_o' - \frac{v}{2b}r_o\right)\left[1 - \frac{5v}{4} + \left(\frac{11}{8} - \frac{15}{16\pi^2}\right)v^2 + \cdots\right]$$

60-3

$$r_{p1} = -\alpha r_o v\left[1 - \frac{v}{4} + \left(\frac{1}{8} - \frac{15}{16\pi^2}\right)v^2 + \cdots\right]$$

$$- \frac{3}{4\pi^2}\alpha b v^2 r_o'\left[1 - \frac{5v}{4} + \left(\frac{15}{8} - \frac{105}{16\pi^2}\right)v^2 + \cdots\right]$$

60-4

These expressions give the first-order perturbations to the motion of the particle in going from z = 0 to z = b. To this must be added the unperturbed motion given by equation 59-3.

Using these equations, it is a straightforward matter to obtain the lens characteristics corresponding to the section of the accelerating column between the centers of two cylinders. As a typical example, the object side focal lengths of the gaps of an accelerating column are plotted in Fig. 17 for the case that the beam energy at the center of the first lens (located at z = 0) is equal to the potential difference between gaps. Curves are given for a/b = .5, 1.0, and 1.5 based upon the foregoing analysis and for a/b less than .25 using the two-cylinder lens characteristics. The focal power of a gap is seen to be nearly independent of the cylinder length for long cylinders, but it decreases rapidly as the length becomes less than a diameter.

The image side focal length f_i is greater than that of the object side by a factor of the square root of the voltage ratio.

$$f_i = \sqrt{1+\nu}\, f_o$$

The unit planes are crossed and lie close together in the negative z direction at a distance nearly equal to the distance of the gap from the origin. Thus, for short

cylinders with the n-th cylinder centered at z = (n-1)b and having a potential V = nV_o, the image side focal length of the n-th gap located at z = $(n-\frac{1}{2})b$ is

$$f_i = \left(1 + \frac{1}{n}\right)^{1/2} f_o$$

and the object and image side unit planes are located respectively at

$$z_o = -nb$$

and

$$z_i = -(n+2)b$$

Focal Properties of a Series of Sections

The focal length of the first n sections of the accelerating column may be determined by successive applications of the lens equations, but the process is rather tedious. When the beam voltage is much greater than the gap voltage difference, it is much simpler to treat the motion of the particles from gap to gap as being a continuous process and to obtain a differential equation for the trajectory.

Using equations 60-3 and 60-4 the change in r and r' in crossing the n-th gap is approximately

$$r_{n+1} - r_n = -\alpha \nu r_n + b r_n'$$

$$r_{n+1}' - r_n' = -\frac{\alpha \nu^2}{2b} r_n - \left(\frac{1}{2} - \alpha\right) \nu r_n'$$

Since the first gap is nearly at zero potential, v is approximately 1/n. Replacing $r_{n+1} - r_n$ by dr/dn, etc., we obtain two simultaneous differential equations

$$\frac{dr}{dn} = -\alpha \frac{r}{n} + br'$$

$$\frac{dr'}{dn} = -\frac{\alpha}{2b} \frac{r}{n^2} - \left(\frac{1}{2} - \alpha\right) \frac{r'}{n}$$

It is to be emphasized that dr/dn represents the change per section in the radial distance of the particle, while r' is the rate of change of r at the center of a cylinder. The two are, therefore, essentially different. r' may be eliminated to give

$$\frac{d^2r}{dn^2} + \frac{1}{2n} \frac{dr}{dn} - \alpha^2 \frac{r}{n^2} = 0$$

which has solutions of the form

$$r = n^k \qquad k = \frac{1}{4} \pm \sqrt{\left(\frac{1}{4}\right)^2 + \alpha^2}$$

or approximately

$$r = n^{\frac{1}{2} + 2\alpha^2} \quad , \quad r = n^{-2\alpha^2}$$

The trajectories are seen to be very nearly parabolic, as is to be expected. Moreover, the focal properties of the column are such that the beam cannot produce more than one real image as it passes down the column.

Putting in boundary conditions, the lens parameters of the section of a column beginning with the m-th gap located at z = mb and ending with the n-th at z = nb are found to be

$$f_o = \frac{mb}{\alpha} \frac{1}{1-\left(\frac{m}{n}\right)^{1/2}}$$

$$Z_o = -mb - 2 f_o \alpha^2 \log \frac{n}{m}$$

$$f_i = \left(\frac{n}{m}\right)^{1/2} f_o$$

$$Z_i = -nb - 2 f_i \alpha^2 \log \frac{n}{m}$$

These equations apply to the case of short cylinders ($a/b \geq \frac{1}{2}$) where the beam has several times the gap voltage as it enters the section starting at z = mb.

Using the lens equations for the first few gaps where the above analysis is not valid, these equations lead to a relatively easy evaluation of the lens characteristics of the entire accelerating column. The results of these calculations are shown in Fig. 17. In each case the object side unit planes are located a few cylinder lengths on the negative side of the origin. Since the focal length of the column is large compared with the distance of the unit plane from the origin, the equivalent lens may be regarded as being situated at the origin.

It is seen from these results that for short cylinder columns, the focal length of the column is generally long enough to be neglected. For longer cylinders, the curves presented permit a fairly accurate estimate of the effective focal length of the accelerating column. Such information is of considerable value in the design of the ion gun as discussed in Chapter V.

VII. CROSS-SECTION OF C^{12} FOR LOW ENERGY PROTONS

Stellar Energy

It has been proposed[24] that the principal source of stellar energy in most stars is a series of reactions in which hydrogen is converted into helium with an evolution of energy corresponding to the mass difference of nearly 1%. This conversion takes place in four steps, making use of the stable isotopes of carbon and nitrogen as catalysts:

$$C^{12} + p \rightarrow N^{13} + \gamma \qquad N^{13} \rightarrow C^{13} + e^{+}$$

$$C^{13} + p \rightarrow N^{14} + \gamma$$

$$N^{14} + p \rightarrow O^{15} + \gamma \qquad O^{15} \rightarrow N^{15} + e^{+}$$

$$N^{15} + p \rightarrow C^{12} + \alpha$$

It was shown by Bethe[24] that, according to our present knowledge, the above process is the only one which is consistent with the known evolution of energy in ordinary stars and with the stellar lifetime. The end products to the other reactions are either energetically forbidden, or occur so infrequently as to be of no consequence. It was further shown that in the course of a stellar lifetime, the carbon and nitrogen catalysts go through the cycle many times so that statistical equilibrium exists among the nuclei involved. Their relative

abundances at the center of a star are, therefore, inversely proportional to their proton capture cross-sections at energies corresponding to the central stellar temperature. The determination of the low voltage cross-section of any one of these catalyzing nuclei, together with a knowledge of their abundance ratios, is thus sufficient to determine the cross-sections of the other nuclei. The measurement of the cross-section of even one of the nuclei involved is, therefore, of considerable importance to the understanding of stellar dynamics.

The energy at which proton capture is most likely in the carbon-nitrogen cycle is determined by the maximum in the product of the Maxwellian velocity distribution among the protons, and the variation with energy of the capture cross-section. This product reaches its maximum at roughly 20kilovolts proton energy for stellar temperatures of 2×10^7 degrees. The cross-sections at this energy are far too small to be measured in the laboratory with existing techniques, so the data obtained at higher energies must be extrapolated to 20 kv. The equipment described in the preceding chapters has been used to extend the measurement of the cross-section of C^{12} down to bombarding energies as low as 100 kev, whereas previously reported data had been taken in the neighborhood of the 453 kilovolt resonance and above. This extension was made possible by the large current of focused protons which could be

obtained from the radio frequency ion source.

The $C^{12}(p,\gamma)N^{13}$ Reaction

The purpose of the experiment to be described is to determine the absolute cross-section of the reaction $C^{12}(p,\gamma)N^{13}$ at the lowest possible bombarding energy. This reaction has been studied by many investigators in the energy region above 300 kev. A well defined resonance exists at 453 kev[25] having a proton width of 35 kev and a gamma-ray width of .63 electron volts. The proton width corresponds to the measured breadth at half maximum of the resonance, while the gamma-ray width, which is calculated from the cross-section at resonance, represents the likelihood that the incident proton will be captured. This information may be used in the dispersion formula to calculate the low energy cross-section, but the results are open to question since they involve a considerable extrapolation from resonance. In the first place, the skirts of higher energy resonances may contribute appreciably to the cross-section. In the second place, the dispersion formula itself is not necessarily valid except in the neighborhood of a resonance.

The N^{13} produced in this reaction has a positron radioactivity with a ten minute half-life. The recent results of Siegbahn and Slatis[26] show that the positron spectrum has a simple Fermi distribution with a maximum

energy of 1.2 Mev. No gamma-radiation other than the annihilation radiation was found, indicating the absence of K-capture or of any other positron groups. The half-life appears to be 10.1 minutes as reported by Siegbahn and Slatis. Earlier investigators quote values between 9.9 and 10.4 minutes. A lower energy positron group has also been reported, but its presence would not affect the cross-section measurements.

The presence of C^{13} in the target does not give rise to any radioactivity since the N^{14} formed by the $C^{13}(p,\gamma)$ reaction is stable. It follows that for every proton captured by C^{12}, there is emitted one positron which is accompanied by no other activity.

Measurement of the Low Voltage Carbon Cross-Section

In order to obtain a measurable yield at as low an energy as possible, a large bombardment current, together with a high counting efficiency in the presence of a low background, is necessary. Using the proton source described in Chapter III, analyzed proton currents of over 200 μa were focused upon an area of about two square millimeters of the target.

Since the counting efficiency for gamma-rays is low, the yield was determined by counting the positrons emitted by the N^{13}. Due to the high background produced by X-rays and sparks during bombardment, it was necessary to

measure the induced radioactivity after the beam was turned off. The target holder shown in Fig. 7 was used for these measurements.

The carbon target, consisting either of a soot deposit or of a graphite cap, was mounted on the water-cooled target sphere. After the bombardment period, the sphere was rotated 180° so as to bring the target before the opening of a mica-window beta-ray counter sealed into the vacuum system. With this arrangement, a large solid angle was obtained with a minimum amount of absorbing material between the target and the sensitive volume of the counter.

The counter used was made by the Radiation Counters Laboratory and was constructed with the sensitive volume reduced in length relative to that of their standard counter. This reduction was accomplished by extending the glass sleeve surrounding the central wire to within a half-inch of the mica window. This modification reduced the background counting rate by a factor of two without appreciably altering the sensitivity of the counter to beta-radiation incident on the window. (See Fig. 20)

To reduce the cosmic ray intensity, the counter was surrounded by 2" of lead on the ends and bottom, 4" on the sides, and $4\frac{1}{2}$" on top. A further reduction in the background was made by using a belt of ten anti-coincidence

counters mounted as shown in Fig. 7. These measures reduced the background counting rate to 5½ counts per minute.

Experimental Results

Counting rates appreciably above background were measured above 100 kev. Bombarding energies were limited to a maximum of 128 kev by the high voltage rectifier arrangement used, and by breakdown of the accelerating column.

The thick target yield curve obtained is shown in Fig. 18. Different runs were made with different bombardment periods and proton currents. In order that all of the results might be plotted on the same curve for comparison, the data has been corrected to give the values which would have been obtained if the bombardment had been made for an infinite length of time using 100 μa of proton current. The probable error indicated represents the statistical fluctuation due to the small numbers of counts recorded. The curve which is drawn through the points has a slope given by the calculated thick target yield obtained from an integration of the Breit-Wigner dispersion formula. In the neighborhood of 100 kev, the thick target yield is proportional to

$$V\left\{1-\left(\frac{V}{2\pi\alpha Z_c}\right)+2\left(\frac{V}{2\pi\alpha Z_c}\right)^2+\cdots\right\}e^{-\frac{2\pi\alpha Z_c}{V}}$$

where v is the velocity of the incident proton, Z is the atomic number of the target nucleus, and α is the fine structure constant. This equation is derived on page 77 and assumes that the stopping cross-section of carbon is constant near 100 kev, and that the energy dependence of the capture cross-section is given by the product of λ^2 and the proton width, the latter being determined essentially by the barrier penetration. The probable error of the data is such that it is not inconsistent with such a curve. Further measurements are in progress to obtain more accurate yield data.

Statistical Errors

Since the counting rates to be measured are only slightly above background, the statistical errors involved are very large and care must be taken to use the data in such a way as to obtain the greatest accuracy. The yield data was obtained by subtracting the expected number of counts due to the background from the number of counts measured in a time T. If the time T were chosen too short, a large error would arise from the smallness of the number of counts observed compared with the random fluctuations. If, on the other hand, the counting time were chosen too long, the statistical fluctuations in the background would introduce an excessive error. An optimum counting time, therefore, exists which will now

be determined together with the associated probable error.

We assume an average exponential decay rate given by

$$\bar{n}_d = \bar{n}_o e^{-\frac{t}{\tau}\log 2} \qquad 73\text{-}1$$

in the presence of an average background rate $\bar{n}_b$. τ is the half-life of the activity and $\bar{n}_o$ is the average initial counting rate. If $\bar{N}_t$ is the average total number of counts observed in the time T, then $\bar{n}_o$ is given by

$$\bar{n}_o = \frac{\log 2}{\tau} \frac{\bar{N}_t - \bar{n}_b T}{1 - e^{-\frac{T}{\tau}\log 2}} \qquad 73\text{-}2$$

The average background rate is accurately known, but the actual number of counts due to background in the time T is uncertain by an amount given by the probable error $.6745\sqrt{\bar{n}_b T}$. Similarly, the fluctuation to be expected in the actual number of counts observed is given by the probable error

$$.6745\left[\bar{n}_b T + \frac{\bar{n}_o \tau}{\log 2}\left(1 - e^{-\frac{T}{\tau}\log 2}\right)\right]^{1/2}$$

The probable error of the sum or difference of two accumulations of random counts is equal to the square root of the sum of the squares of the separate errors. Thus, the probable error of the average number of counts

above background is

$$.6745\left[2\bar{n}_b T + \frac{\bar{n}_o \tau}{\log 2}\left(1 - e^{-\frac{T}{\tau}\log 2}\right)\right]^{1/2}$$

The relative probable error is obtained by dividing this by the average number of counts above background

$$\mathcal{E} = .6745\,\frac{\left[2\bar{n}_b T + \frac{\bar{n}_o \tau}{\log 2}\left(1 - e^{-\frac{T}{\tau}\log 2}\right)\right]^{1/2}}{\frac{\bar{n}_o \tau}{\log 2}\left(1 - e^{-\frac{T}{\tau}\log 2}\right)}$$

We wish to choose T so as to make the relative error a minimum. Setting the derivative equal to zero results in the equation

$$\frac{\bar{n}_o}{\bar{n}_b} = 2\,\frac{e^x - 1 - 2x}{1 - e^{-x}} \qquad x = \frac{T}{\tau}\log 2$$

The corresponding value of the minimum error is given by

$$\mathcal{E}_{min} = .6745\left[\frac{\log 2}{2\bar{n}_b \tau}\,\frac{e^x - 1 - x}{(e^x - 1 - 2x)^2}\right]^{1/2}$$

The optimum counting time T_o, expressed in half-lives, is determined by the initial decay rate divided by the background counting rate, and is plotted in Fig. 19. For initial counting rates equal to the background or less, the minimum error is obtained if counts are recorded for approximately two half-lives.

The relative probable error $\mathcal{E}_{min}$ corresponding to the optimum counting time is also plotted in Fig. 19 for various background counting rates. Since the average initial counting rate cannot be determined from a single measurement, the assumption is made in determining the error that the observed initial counting rate is approximately equal to the average value.

Calculation of the Absolute Value of the Cross-Section

In order to obtain the thick target yield in disintegrations per proton, a number of corrections must be made. The initial decay rate given by equation 73-2 must be increased by a factor

$$\frac{1}{1 - e^{-\frac{t}{\tau}\log 2}}$$

to account for the fact that an equilibrium concentration of N^{13} nuclei was not attained during the finite bombardment time t.

A factor f will be used to represent the fraction of the disintegration positrons which are registered by the counting circuits. This factor takes into account the solid angle subtended by the counter, the counter efficiency, and the fraction of the positrons which are missed due to absorption in the mica window and to the N^{13} nuclei which leave the target before disintegrating. Because of the low counting rates involved, a resolving

time correction is not necessary. The equilibrium decay rate is, therefore, given by

$$\frac{\log 2}{\tau f} \frac{\bar{N}_t - \bar{n}_b T}{\left(1 - e^{-\frac{T}{\tau}\log 2}\right)\left(1 - e^{-\frac{\xi}{\tau}\log 2}\right)} \qquad 76\text{-}1$$

and the thick target yield by

$$Y = \frac{e}{I} \frac{\log 2}{\tau f} \frac{\bar{N}_t - \bar{n}_b T}{\left(1 - e^{-\frac{T}{\tau}\log 2}\right)\left(1 - e^{-\frac{\xi}{\tau}\log 2}\right)} \qquad 76\text{-}2$$

where I and e are the analyzed proton current and the electron charge respectively.

The cross-section is calculated from the thick target yield by a method which makes use of the fact that in the neighborhood of 100 kev, the stopping cross-section of air (and consequently that of carbon also) is very nearly independent of the proton energy.

The proton capture cross-section σ for protons of velocity v and energy E is proportional to the product of λ^2 and the barrier penetration factor.

$$\sigma \sim \lambda^2 e^{-\frac{2\pi\alpha Z c}{v}} \quad \text{or} \quad \sigma = a \frac{e^{-\frac{b}{v}}}{v^2} \qquad 76\text{-}3$$

While this formula cannot be used to obtain the absolute value of the cross-section, it may be expected to represent the variation with energy of the cross-section over a limited energy range.

The thick target yield is given by

$$Y = n\int \sigma\, dx = n\int_{\epsilon}^{0} \sigma \frac{d\epsilon}{\frac{d\epsilon}{dx}} = -\frac{n}{\frac{d\epsilon}{dx}}\int_{0}^{\epsilon} \sigma\, d\epsilon = -\frac{mn}{\frac{d\epsilon}{dx}}\int_{0}^{v} \sigma v\, dv$$

$$= \frac{mna}{\left(-\frac{d\epsilon}{dx}\right)}\int_{0}^{v} e^{-\frac{b}{v}} \frac{dv}{v} \qquad 77\text{-}1$$

where m is the proton mass and n is the number of C^{12} nuclei per cc, and a and b are defined by equation 76-3. A rapidly converging series is obtained for this integral by successive integrations by parts

$$Y = \frac{mna}{\left(-\frac{d\epsilon}{dx}\right)} \frac{v}{b} e^{-\frac{b}{v}} \left\{1 - \frac{v}{b} + 2\frac{v^2}{b^2} - 6\frac{v^3}{b^3} + \cdots\right\} \qquad 77\text{-}2$$

Since v/b = .0531 for 100 kev protons, it is sufficient to retain only the first two terms of the series. The thick target yield, expressed in disintegrations per proton, is thus given by

$$Y = \frac{mn\sigma}{\left(-\frac{d\epsilon}{dx}\right)} \frac{v^3}{b}\left(1 - \frac{v}{b}\right) \qquad 77\text{-}3$$

or

$$\sigma = \frac{\epsilon Y}{m\frac{v^3}{b}\left(1 - \frac{v}{b}\right)} \qquad 77\text{-}4$$

where $b = 2\pi\alpha cZ$ and ϵ is the atomic stopping power of the carbon target. Livingston and Bethe[27] give the atomic

stopping cross-section for air at 100 kev to be 1.51×10^{-14} cm^2 volt. They believe that this figure is correct to within 10%, and there appears to be no better data available. The stopping cross-section of carbon is smaller by a factor of approximately .96. A value of 1.45×10^{-14} cm^2 volt has been used in calculating the carbon cross-section near 100 kev.

Determination of the Fraction of Disintegrations Counted

The factor f representing the fraction of disintegrations which are observed will now be discussed. The positron spectrum measured by Siegbahn and Slatis[16] shows that less than 1% of the positrons have energies below 100 kev. The mica window of the counter has a thickness of 2 mg/cm^2 which is capable of stopping only a small fraction of the positrons having this energy. Absorption in the counter window may, therefore, be neglected.

There is considerable evidence that a negligible amount of N^{13} leaves the target. Roberts and Heydenburg[28] estimate that the counting rate is decreased about 10% by the loss of active nitrogen. On the other hand, in their investigation of the carbon reaction above 300 kev, Lauritsen, Lauritsen and Fowler found no evidence for any such effect. In order to reduce any loss of nitrogen in the low voltage experiments, the target sphere was water-

cooled. As may be seen from Fig. 18, the same yields were obtained within experimental error for targets made of graphite, soot, and the black deposit formed on the brass surface of the sphere by prolonged bombardments. This is further evidence that a negligible amount of active nitrogen leaves the target.

The effective aperture and counter efficiency were examined in the experiment illustrated in Fig. 20. The beta-particles from a Ra D source were collimated by a lead canal so as to produce a beam having a width of about one millimeter. The alpha-particles were removed by a thin aluminum foil so that the resulting beam consisted only of beta-particles having an energy comparable to that of the N^{13} positrons. The source and collimator could be rotated about an axis perpendicular to the beam and to the axis of the counter. This axis was located 3 mm from the plane of the periphery of the mica window so that the particles from the beam entered the counter at the same angles as did the N^{13} positrons. The counting rate was measured as a function of the angle of incidence of the beam, giving the curves shown in Fig. 20. Three counters were measured in this fashion. The special low background counter used in the measurements of the carbon reaction and having 13 mm of exposed central wire was compared with two standard counters having 50 mm of

exposed wire.

The maximum counting rate is nearly the same for each of the standard counters but is slightly less for the special low background counter. This difference indicates that the active volume of the low background counter is sufficiently shallow that an appreciable fraction of the beta-particles pass through without being counted. It is also to be noted that the curve of the low background counter rises more sharply than do those of the standard counters, indicating that the former counter is filled with a slightly higher gas pressure. The curve for the low background counter reaches half sensitivity at an angle of 27^{o} corresponding to a path length within the counter of 7 mm. Since the active length of this counter is likely to be not much greater than the 13 mm length of exposed center wire, it is not unreasonable that an appreciable fraction of the particles pass through this counter without being counted. On the other hand, particles entering along the axis of the standard counters are almost certain to be counted.

The curve for the low background counter represents its counting efficiency as a function of the angle of incidence, the maximum of the standard counter curves corresponding to 100% efficiency. Using this curve as a weight function and integrating over all angles gives the

effective aperture of the counter. A solid angle of 3.3 steradians is thus obtained corresponding to a counting efficiency of 26%. The curves of Fig. 20, and hence the efficiency, were found to be nearly independent of the counter voltage within the limits of the plateau.

The yield at 100 kev obtained from Fig. 18 results in a cross-section of 1.5×10^{-34} cm^2 using equations 76-2 and 77-4, with a stopping cross-section of 1.45×10^{-14} cm^2 volt and a counting fraction of 26%.

Experimental Errors

A number of sources of error are involved, most of which may be placed within fairly well defined limits. Certain other sources of error are believed to be small but are not easily estimated; these are all such as to give too small a computed cross-section.

Examination of Fig. 18 shows that the yield is very sensitive to the proton energy; a 1% error in the voltage measurement is equivalent to a 10% error in the yield. In addition to the voltage calibration described on page 7, a Type K potentiometer was used to measure the voltage developed across a precision resistor by the current from the 120 megohm stack of high voltage resistors. The two methods of calibration agreed within 1%. The latter, being the more accurate, was used in

plotting the yield curve. Both calibrations depend upon the accuracy of the 20 megohm precision resistor which was used as a standard to measure the 120 megohm stack. This stack was constructed from 1% accuracy 1 megohm wire-wound resistors and the measurement of each section agreed within a few tenths of one percent of the nominal value. The voltage was continuously adjusted during each run so as to maintain a steady value. Corona currents to junctions between the sections of the 120 megohm stack were eliminated by maintaining large clearances between the stack and other conductors, and by wrapping the junctions with dental dam. It is believed that errors in cross-section due to inaccuracy in the voltage measurement amount to less than 10%.

The proton current meter was calibrated and introduces negligible uncertainty.

The stopping cross-section for carbon may be in error by 10% according to Livingston and Bethe[27].

The measurement of the fraction of counts recorded would appear to introduce only a few percent error.

Blank runs have been made using the brass target sphere as a target instead of carbon. It was necessary to install a dry ice trap in the vacuum system to reduce the deposition of carbon upon the brass. The trap

decreased the pressure indicated by the ion gage by a factor of four, and bombardment periods of over ten minutes could be used without forming a detectable carbon deposit. One such blank run is shown in Fig. 18.

The positron radiation is not believed to be accompanied by any other kind of radioactivity which could cause spurious counts. The counter pulses were watched on an oscilloscope to check on the possibility of counter breakdown. The counter plateau was checked at frequent intervals to make sure that the counter was performing properly. The negative results obtained from the blank runs further indicate that the counters were functioning properly.

The guard-ring potential of the target holder was adjusted so as to be well above the value required to return all secondary electrons to the target.

Loss of nitrogen from target and oil contamination are both believed to cause negligible error. Both of these effects would give too small a cross-section.

The 1% fraction of C^{13} nuclei in the target may be neglected in comparison with the other errors.

The statistical errors involved are indicated in Fig. 18. If it is assumed that the slope of the thick target yield curve is given correctly by equation 77-2 over the energy range explored, the cross-section at

100 kev may be evaluated with an uncertainty of about 20% due to the statistics.

Conclusion

The cross-section at 100 kev was calculated to be 1.5×10^{-34} cm^2 but is uncertain by a factor of about 1.4. This cross-section is three times as large as that obtained from the dispersion formula using recent data[25] for the shape of the 453 kev resonance. This is consistent with the observation that the data points of Fig. 18 would seem to indicate a less rapidly varying yield than the calculated thick target yield curve which is drawn through them.

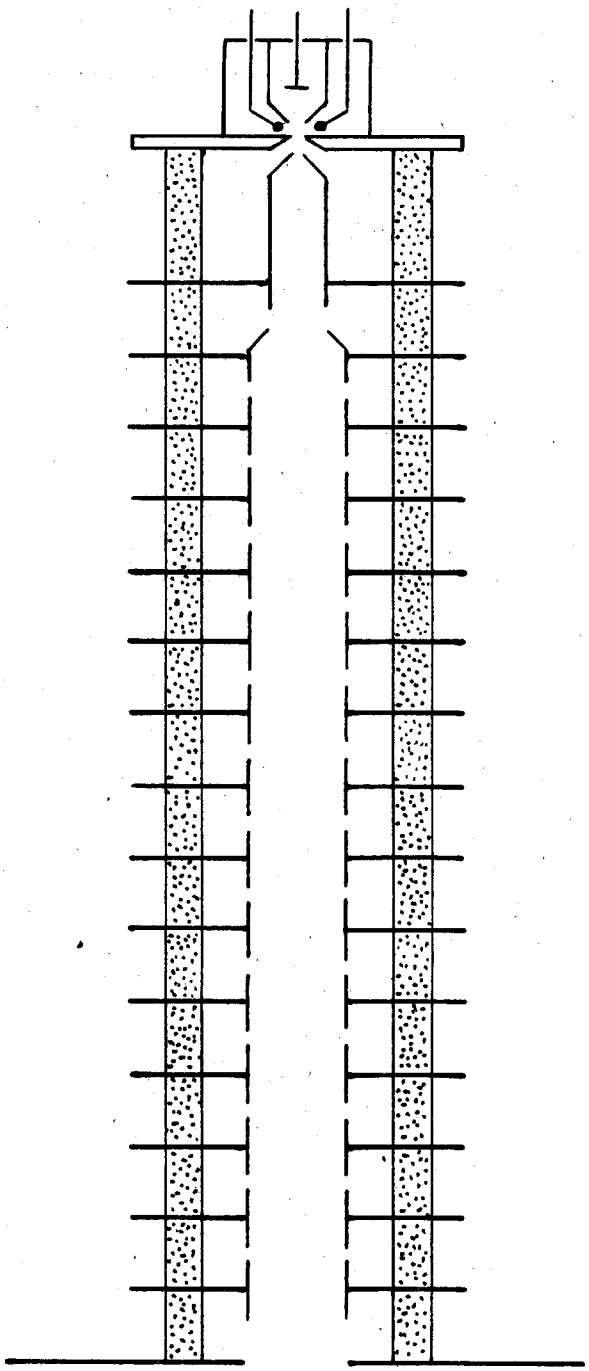

Fig. 1 CONSTANT VOLTAGE ACCELERATING SYSTEM

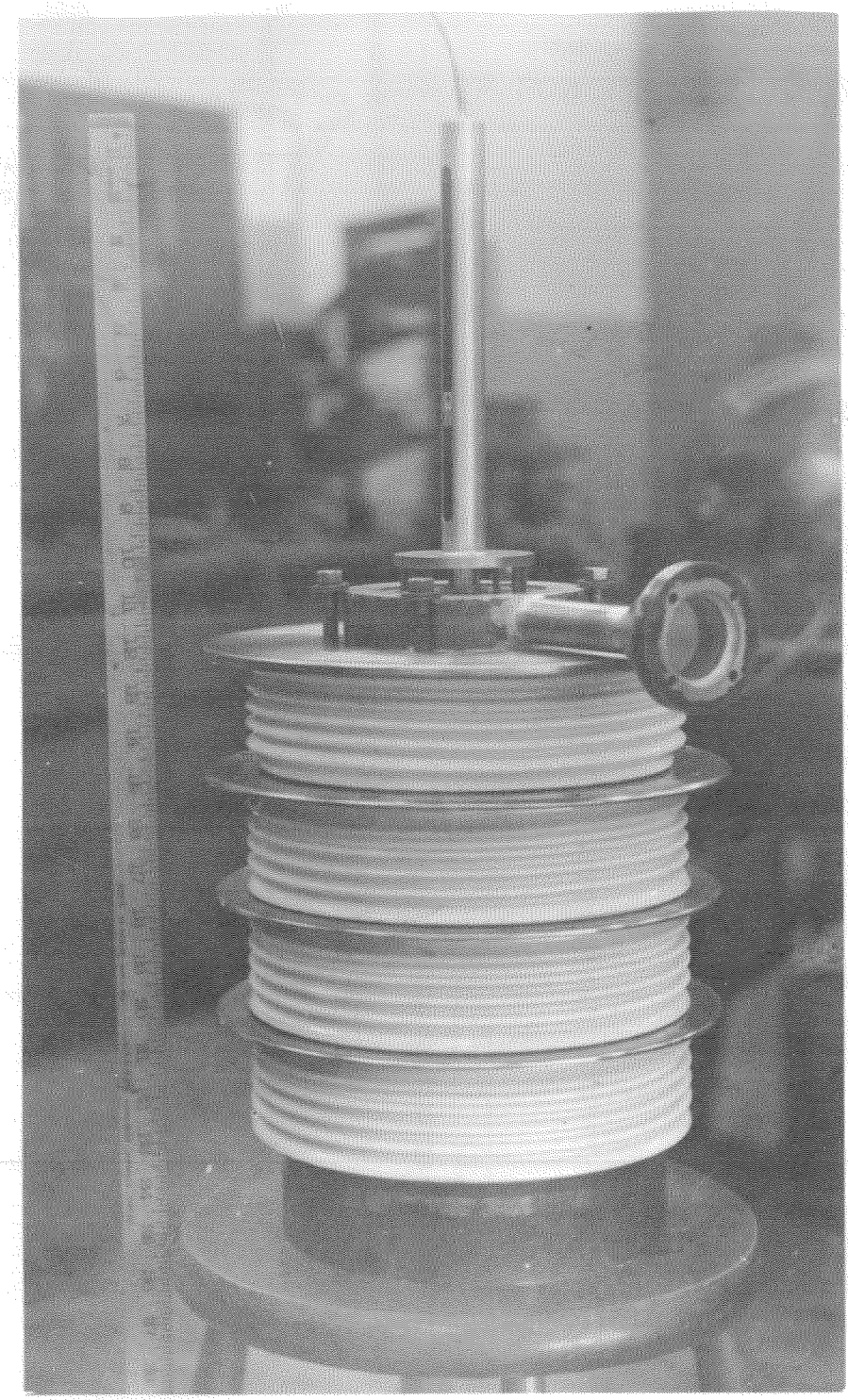

Fig. 2. Ion Source and Accelerating Column.

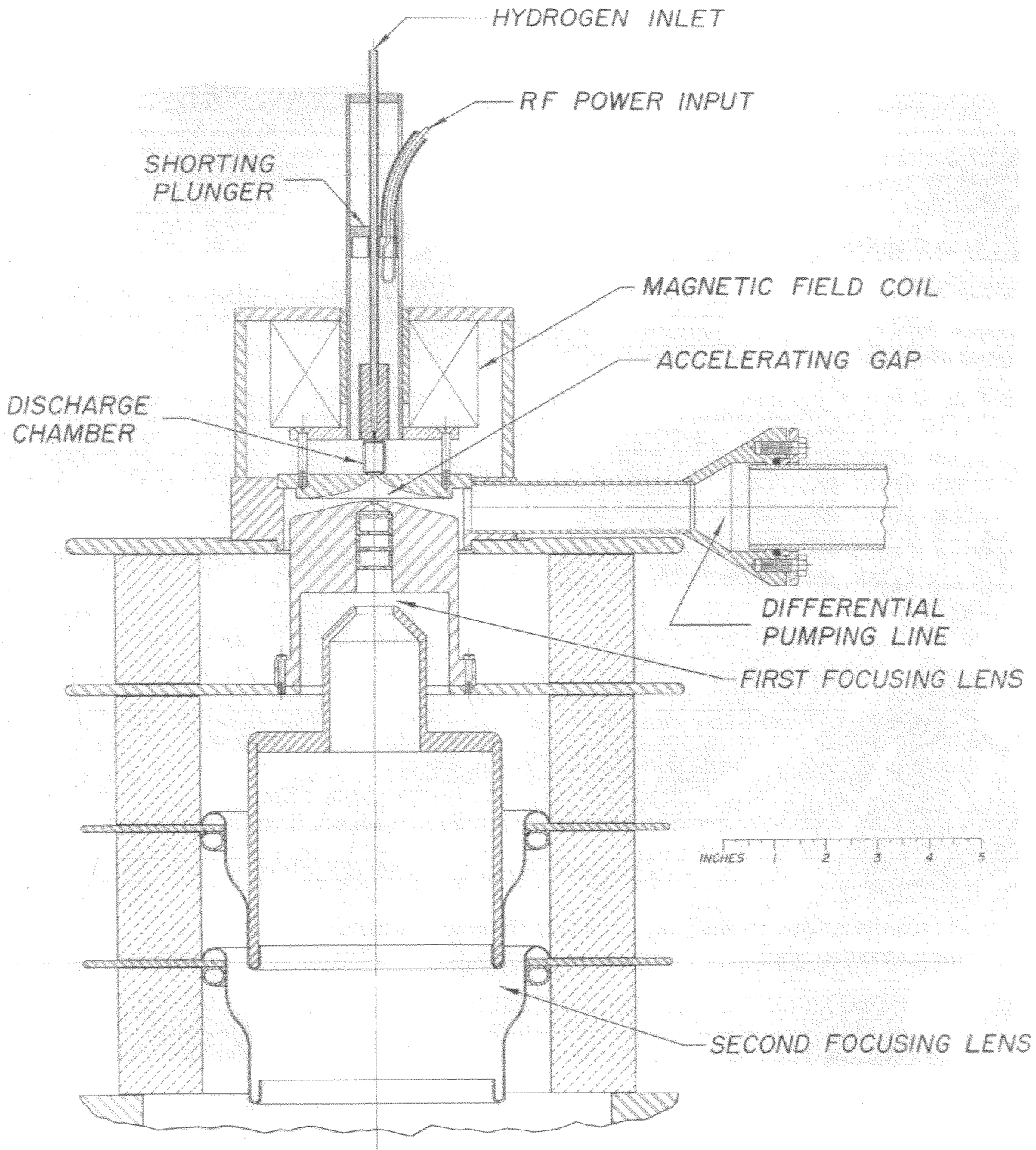

Fig. 3. Radio Frequency Ion Source and Accelerating Electrode System.

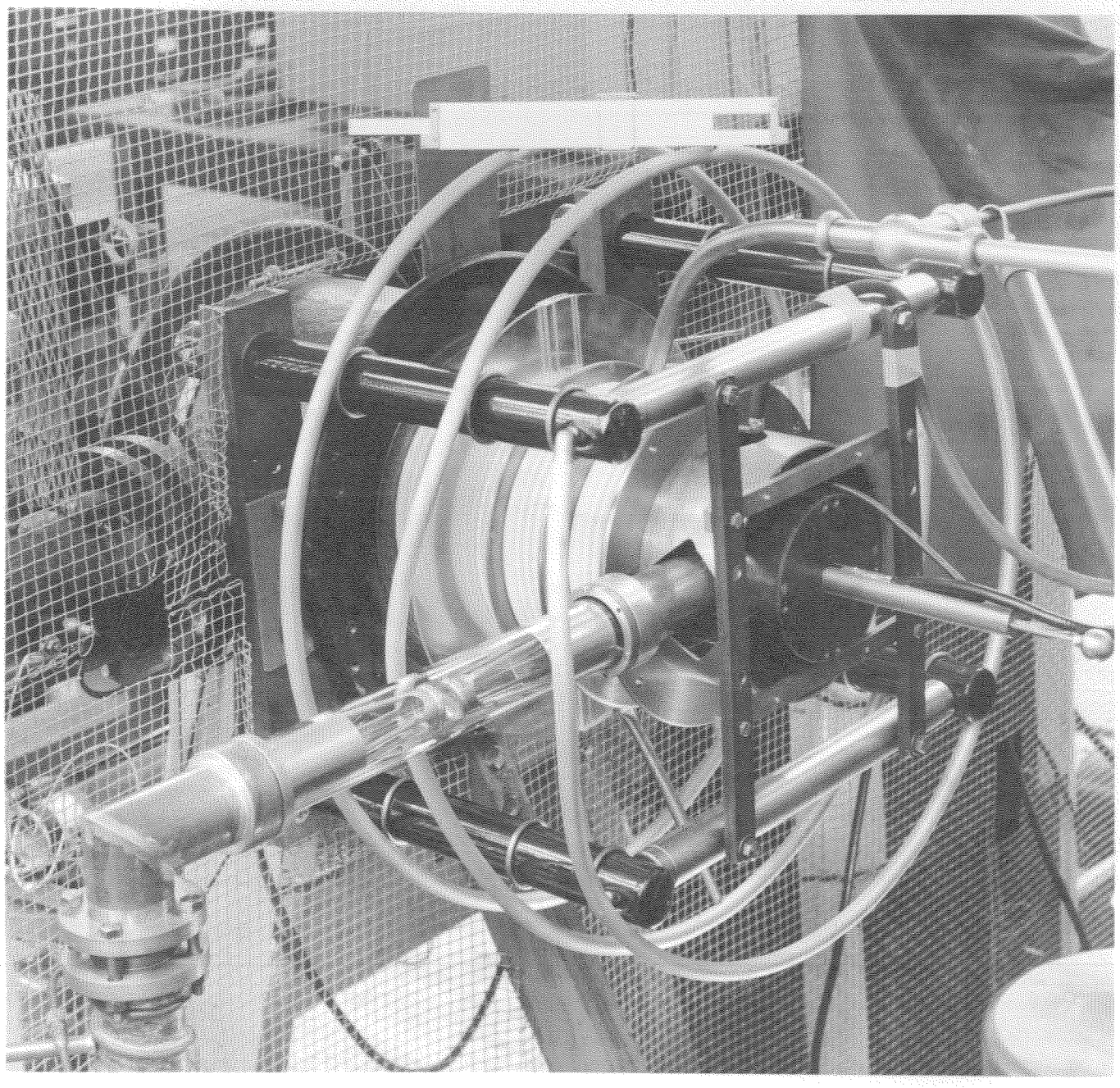

Fig. 4. Low Voltage Accelerator Completely Assembled.

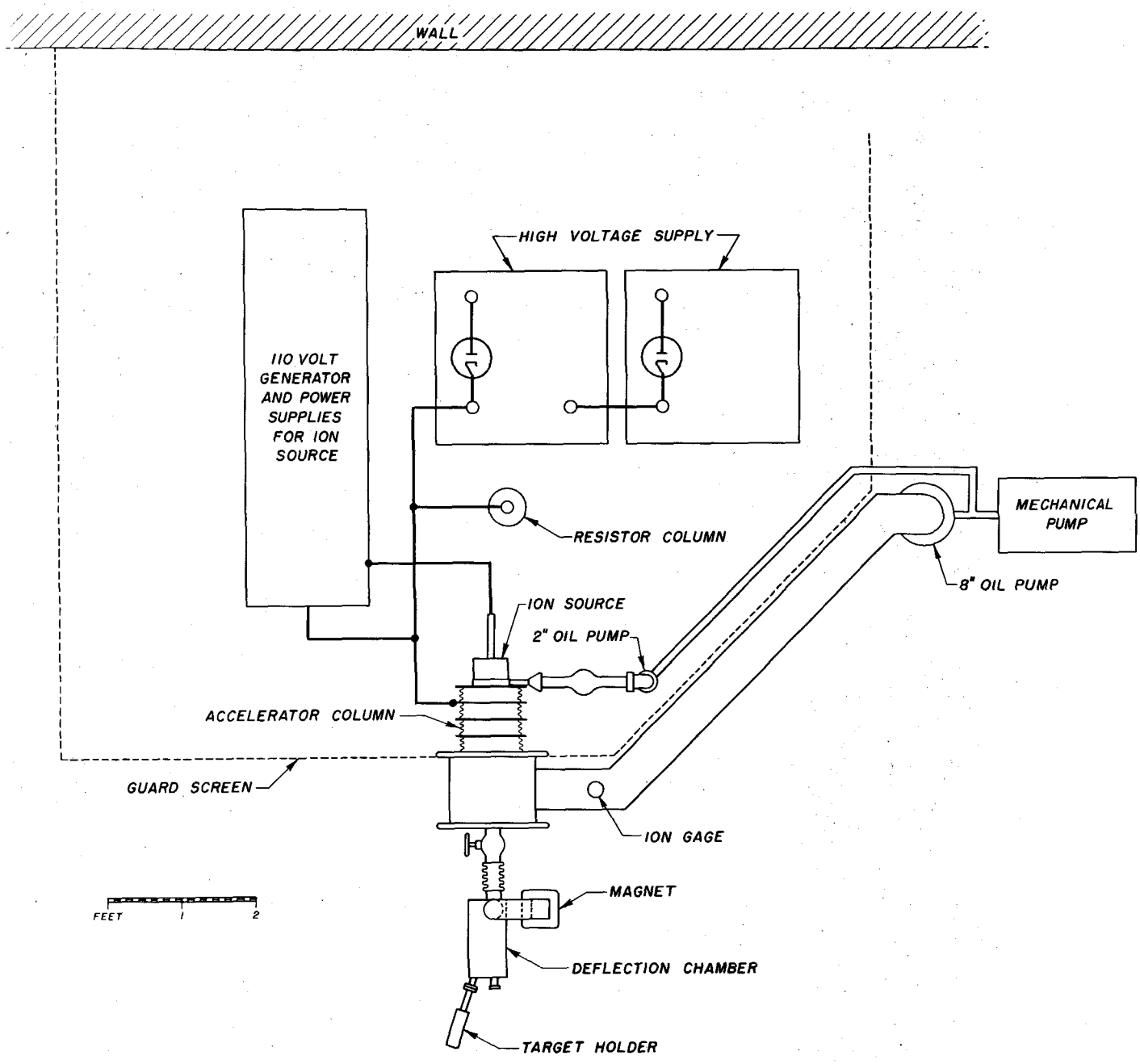

Fig. 5. Plan View of Experimental Set-up.

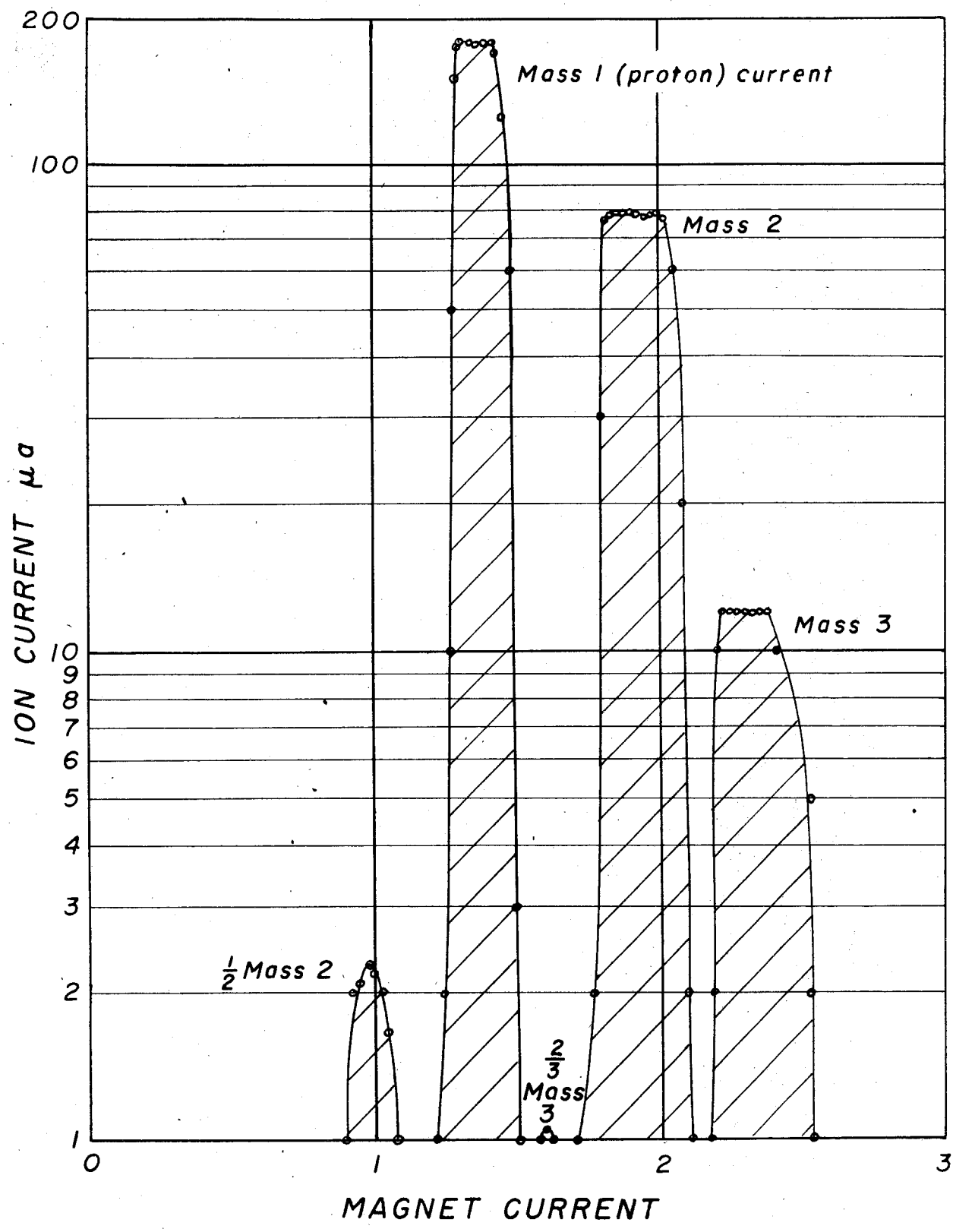

Fig. 6 MAGNETIC ANALYSIS OF THE ION BEAM

Current collected through a 5/8" diameter aperture is plotted against magnetic deflection current. The two small peaks are due to fragments of mass two and three ions which were scattered by residual gas after passing through the accelerator.

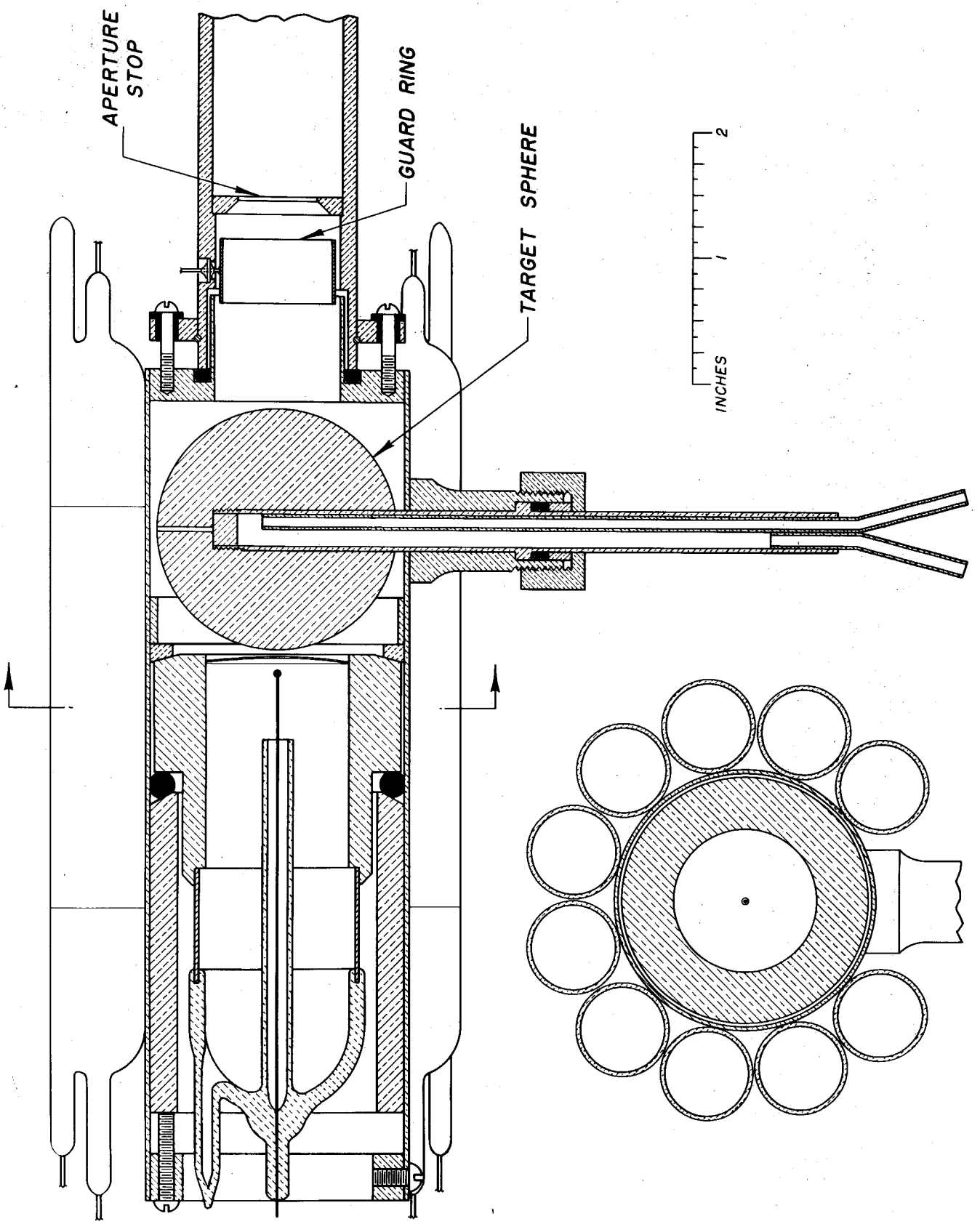

Fig. 7. Target Holder.

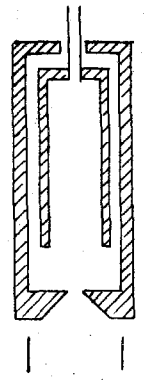

Oliphant and Rutherford
High Voltage Ion Source

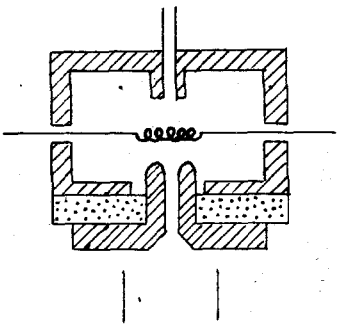

Crane, Lauritsen and
Soltan Proton Source

Fig. 8a Early High Voltage Ion Sources

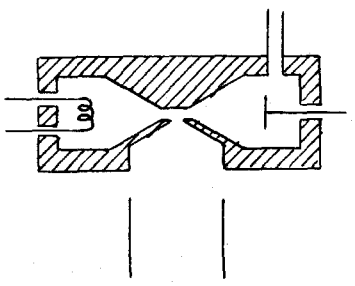

Capillary Arc

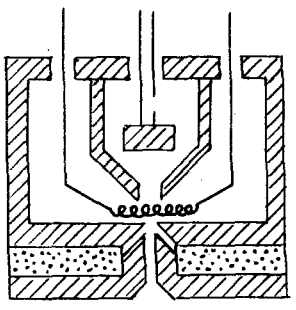

Zinn-Type Source

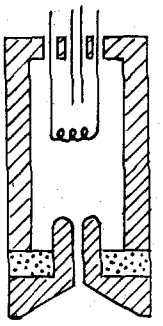

Carnegie Source

Fig. 8b Low Voltage Arc Discharge Proton Sources

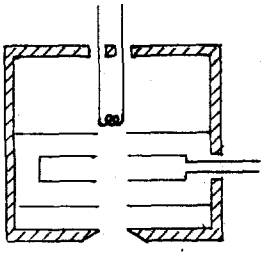

Finkelstein
Proton Source

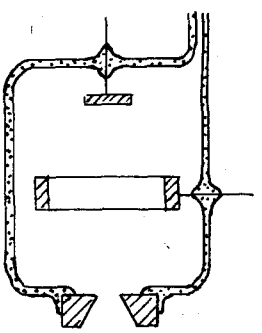

Imperial College
Cold Cathode Source

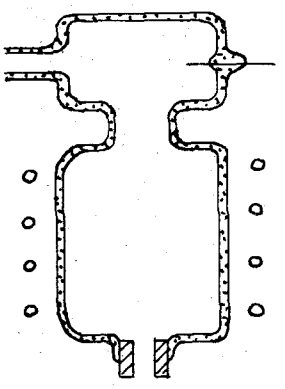

British R.F.
Ion Source

Fig. 8c Ion Sources Using an Axial Magnetic Field

Fig. 8 TYPES OF ION SOURCES

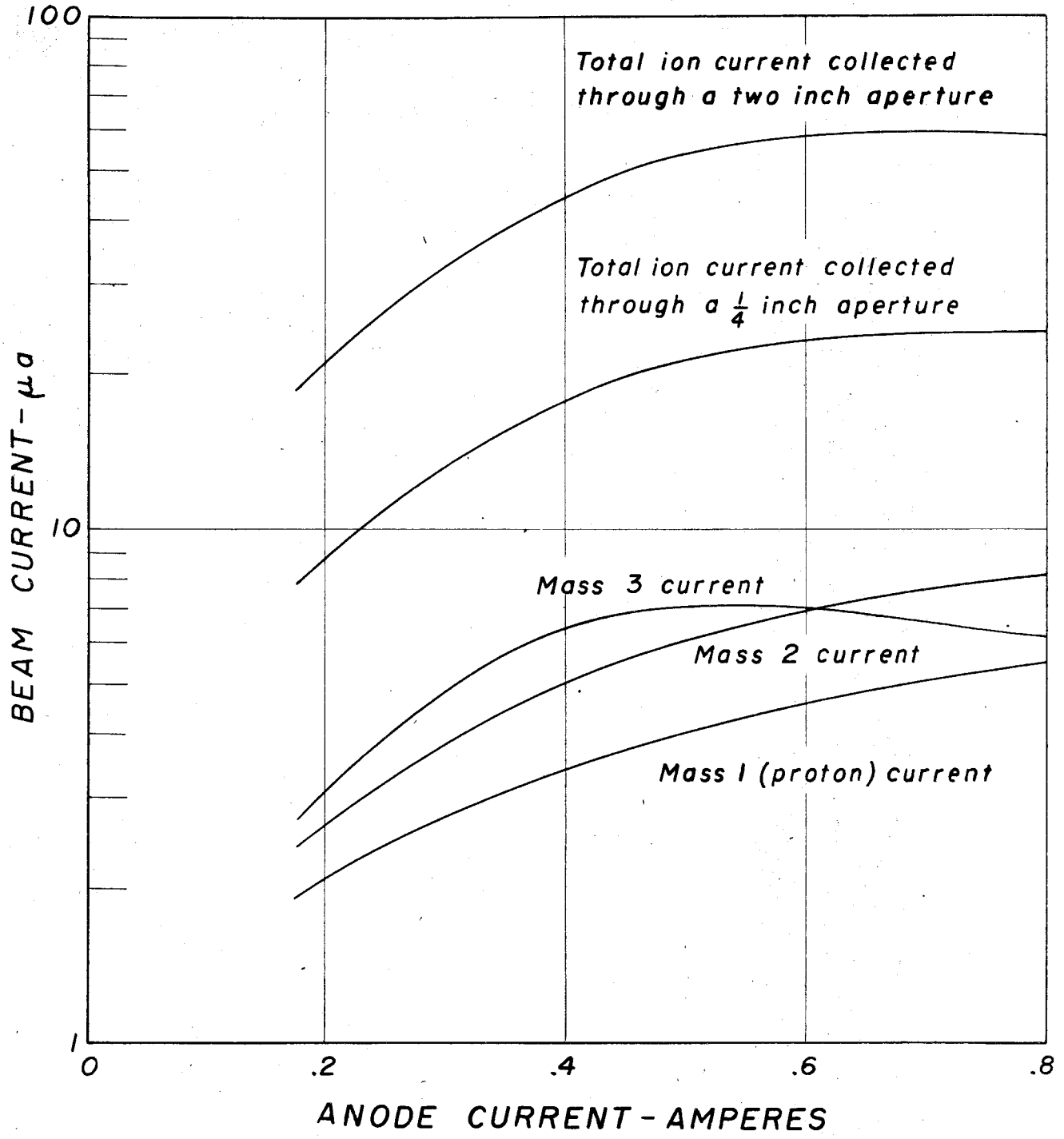

Fig. 9 BEAM CURRENT FROM ZINN SOURCE WITH PROBE

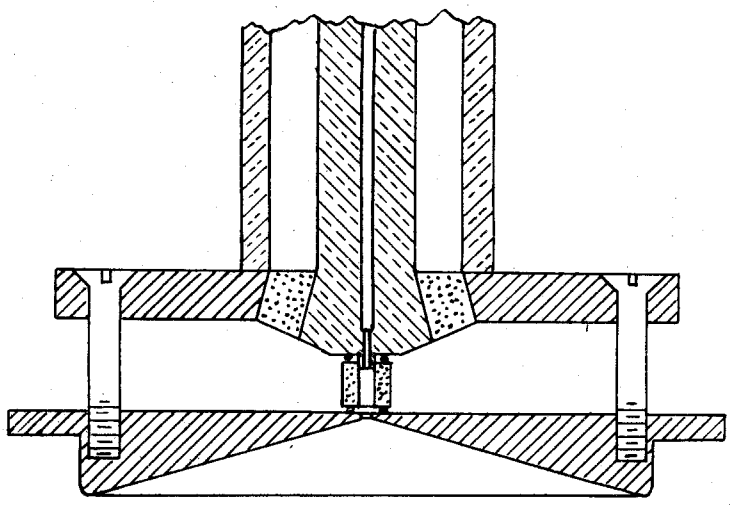

Fig. 10a Quartz Capillary Discharge Chamber

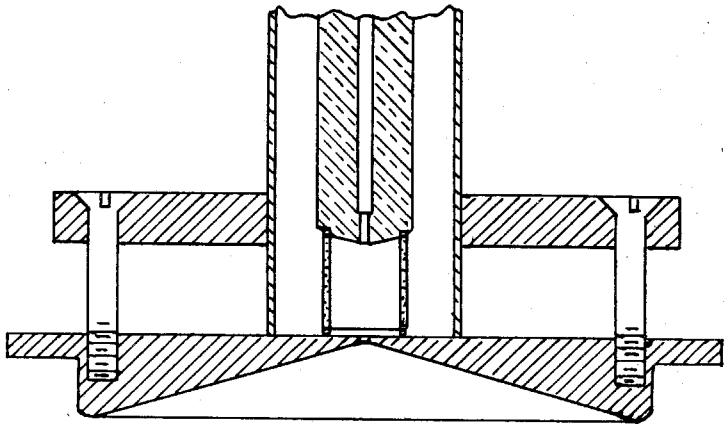

Fig. 10b Quartz Cylinder Discharge Chamber

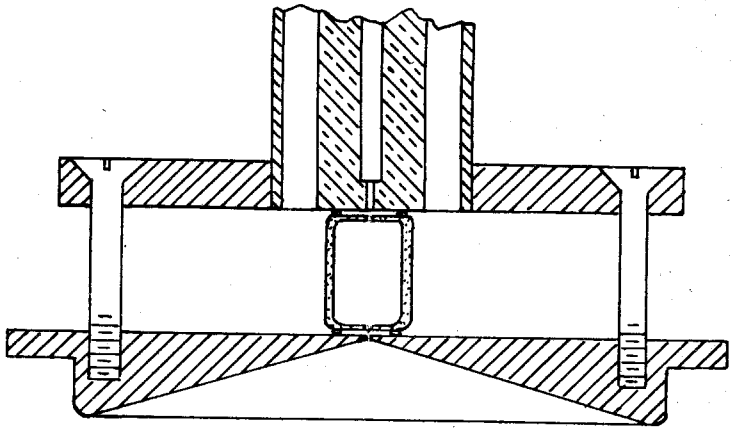

Fig. 10c Barrel-Shaped Quartz Discharge Chamber

Fig. 10 EXPERIMENTAL RADIO FREQUENCY ION SOURCES

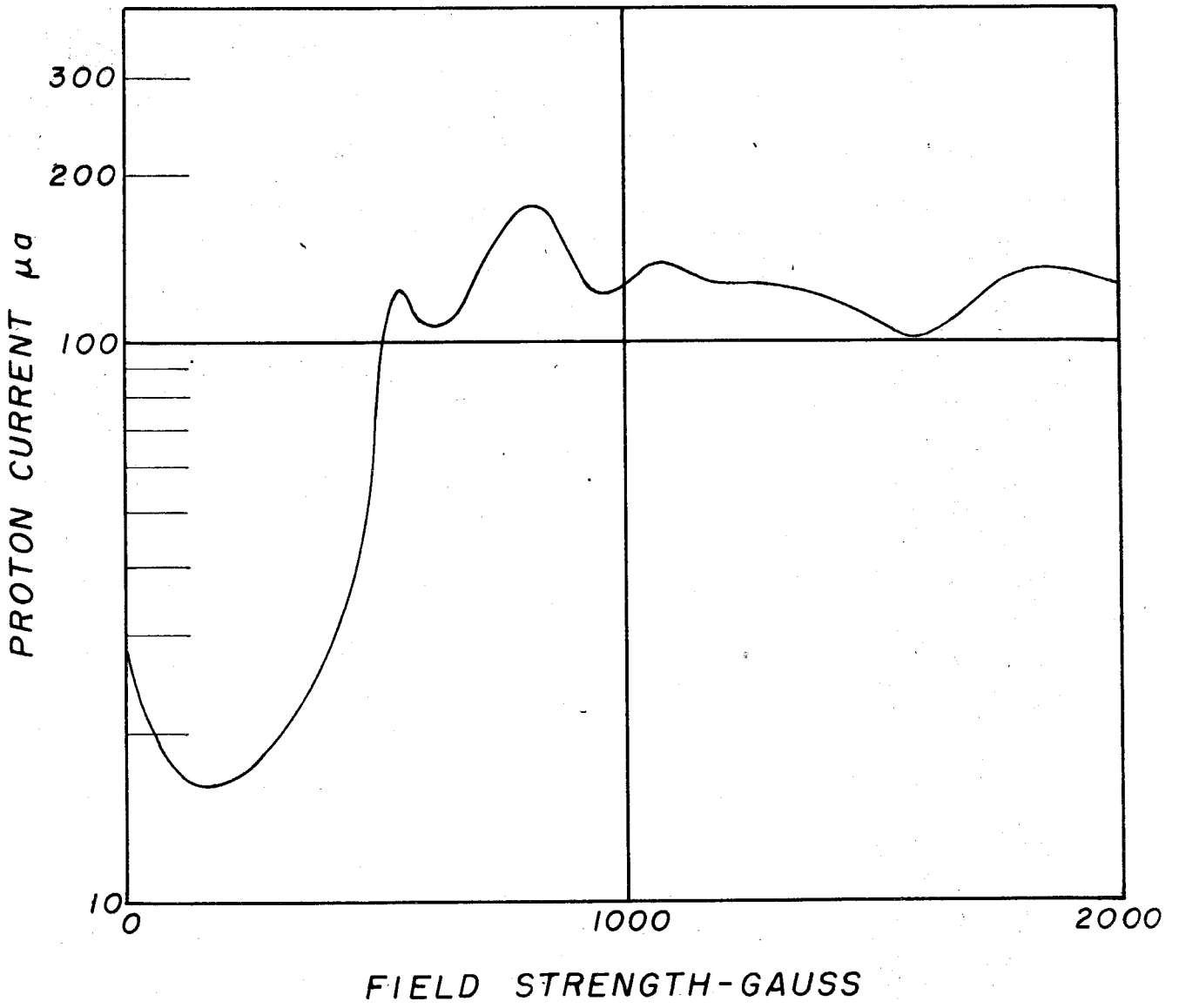

Fig. 11 EFFECT OF AXIAL MAGNETIC FIELD ON PROTON CURRENT

A typical yield curve is shown above for a discharge chamber having a .040" diameter exit hole. The details of the curve appear to depend upon the discharge chamber geometry, the frequency, and the uniformity of the magnetic field.

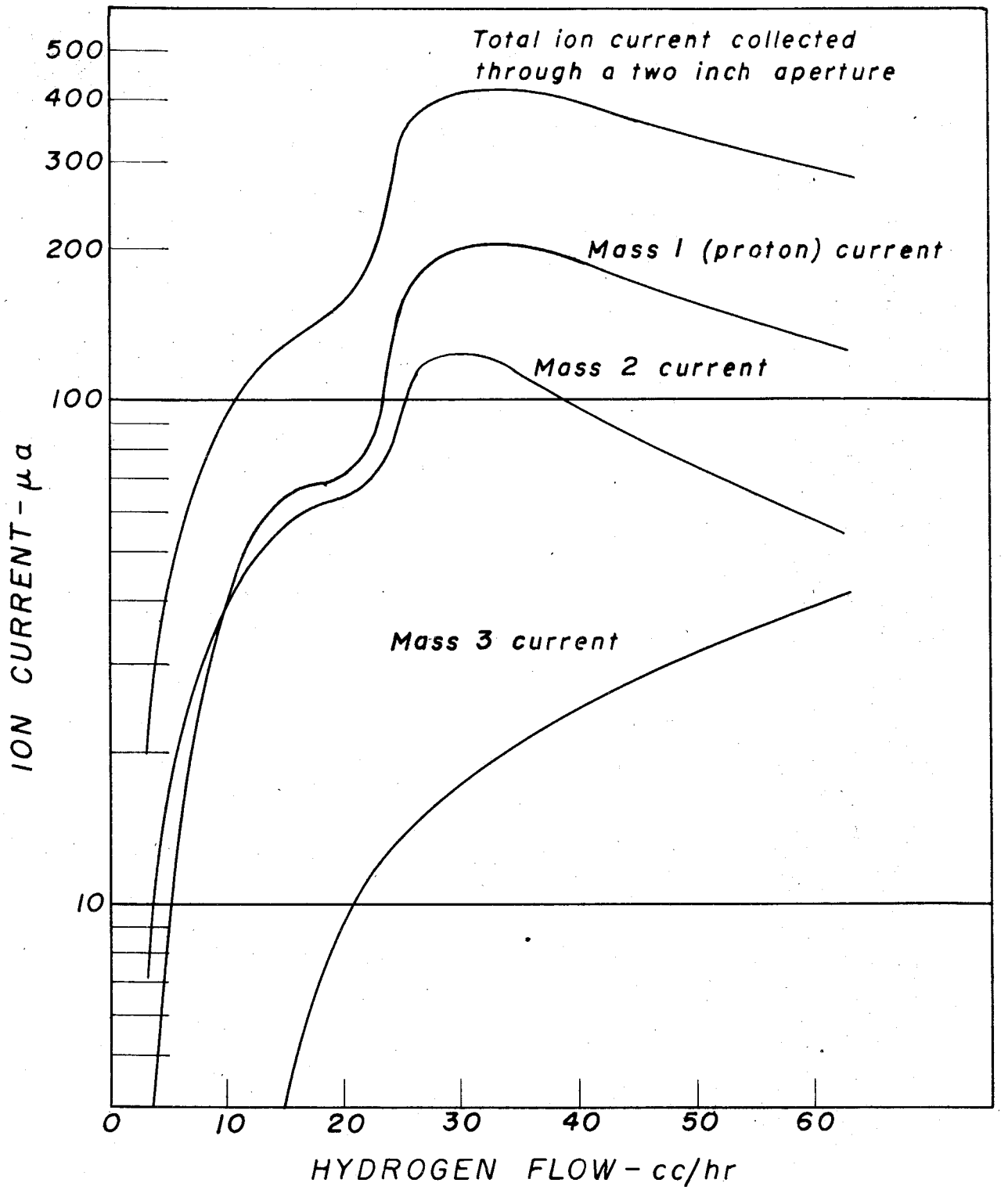

Fig. 12 VARIATION OF ION YIELD WITH HYDROGEN FLOW

Discharge chamber is pyrex, .31" diameter, .42" long inside, with a .040" diameter exit hole. Approximately 50 watts of 450 mc/sec radio frequency power being supplied. Axial magnetic field adjusted for maximum proton current at each measurement.

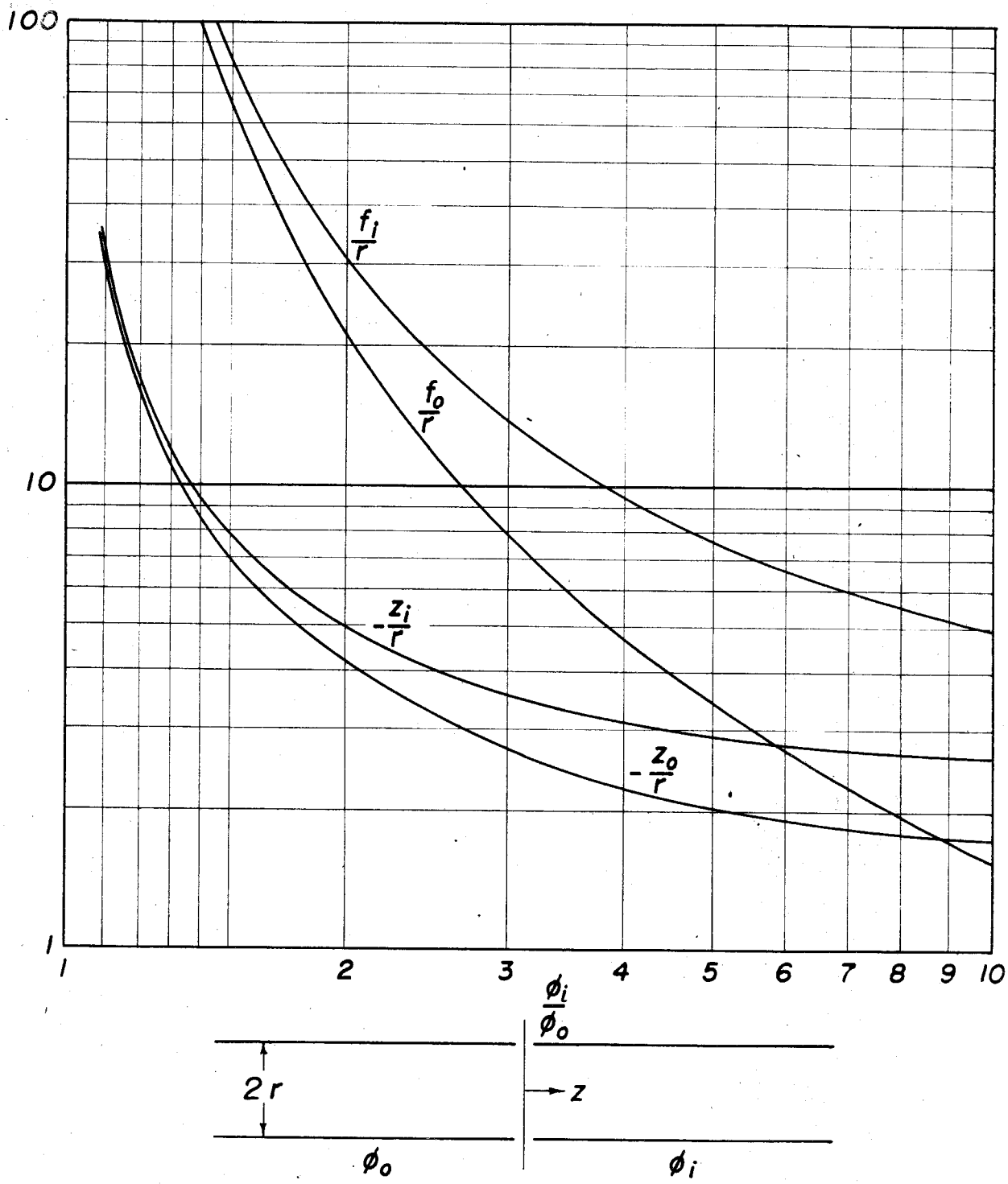

Fig. 13 FOCAL PROPERTIES OF THE TWO-CYLINDER ELECTROSTATIC LENS

f_o and f_i are the object and image side focal lengths. The unit planes are located at z_o and z_i.

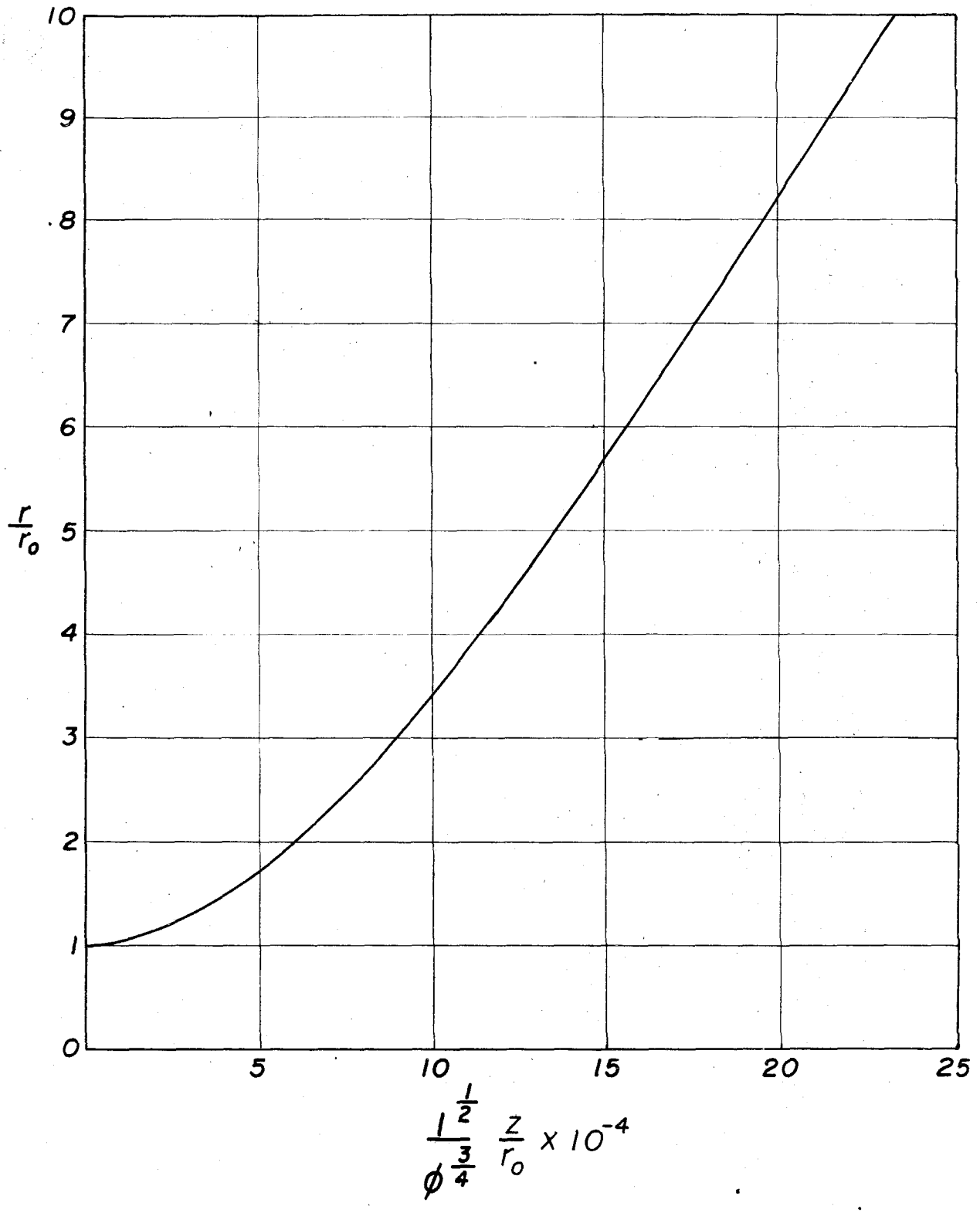

Fig. 14 SPACE-CHARGE SPREADING OF ION BEAMS

The curve gives the spreading due to space-charge repulsion of a beam of charged particles which initially are moving parallel to each other in a beam of radius r_o. The effective proton current I is expressed in μa, and the beam energy ϕ in Mev.

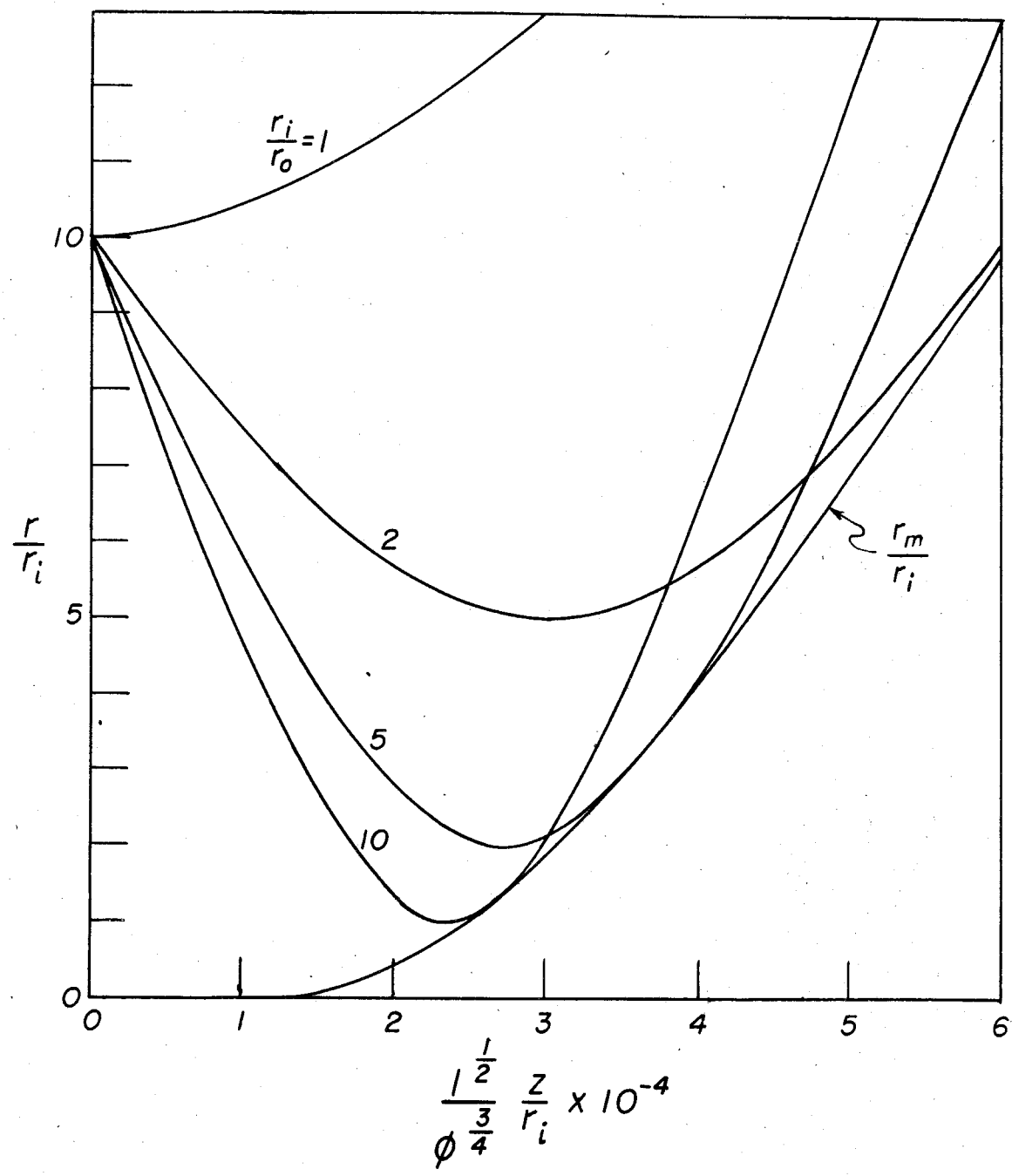

Fig. 15 ION BEAM TRAJECTORIES UNDER INFLUENCE OF SPACE-CHARGE

The trajectory of ion beams having an initial radius r_i and varying degrees of convergence are shown. The radius of the beam reaches a minimum value r_o and then diverges again. The envelope gives the minimum radius r_m which an ion beam may have after traveling a distance z from the place where it had a radius r_i. The effective proton current I is expressed in μa and the beam energy ϕ in Mev.

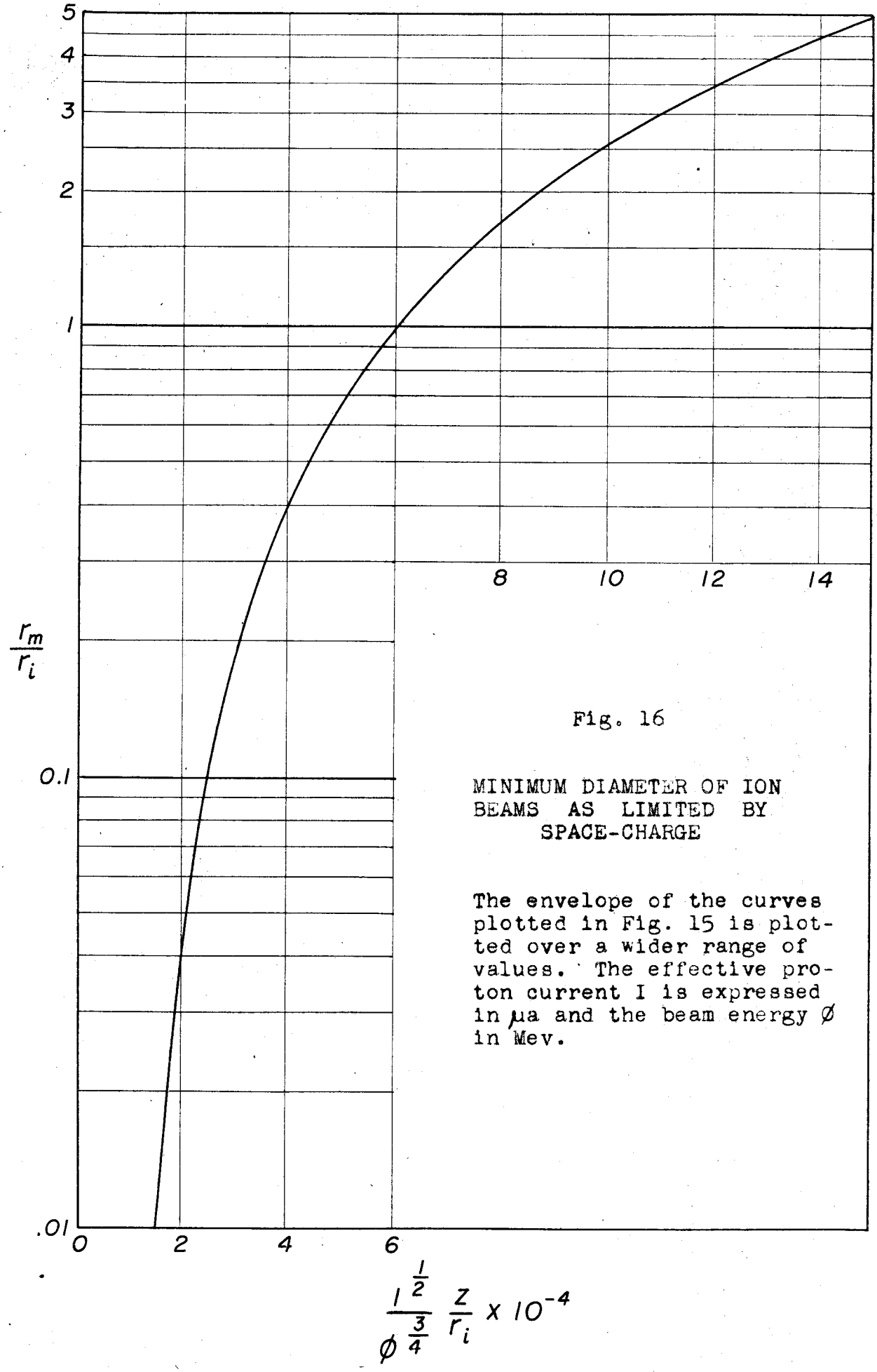

Fig. 16

MINIMUM DIAMETER OF ION BEAMS AS LIMITED BY SPACE-CHARGE

The envelope of the curves plotted in Fig. 15 is plotted over a wider range of values. The effective proton current I is expressed in μa and the beam energy Ø in Mev.

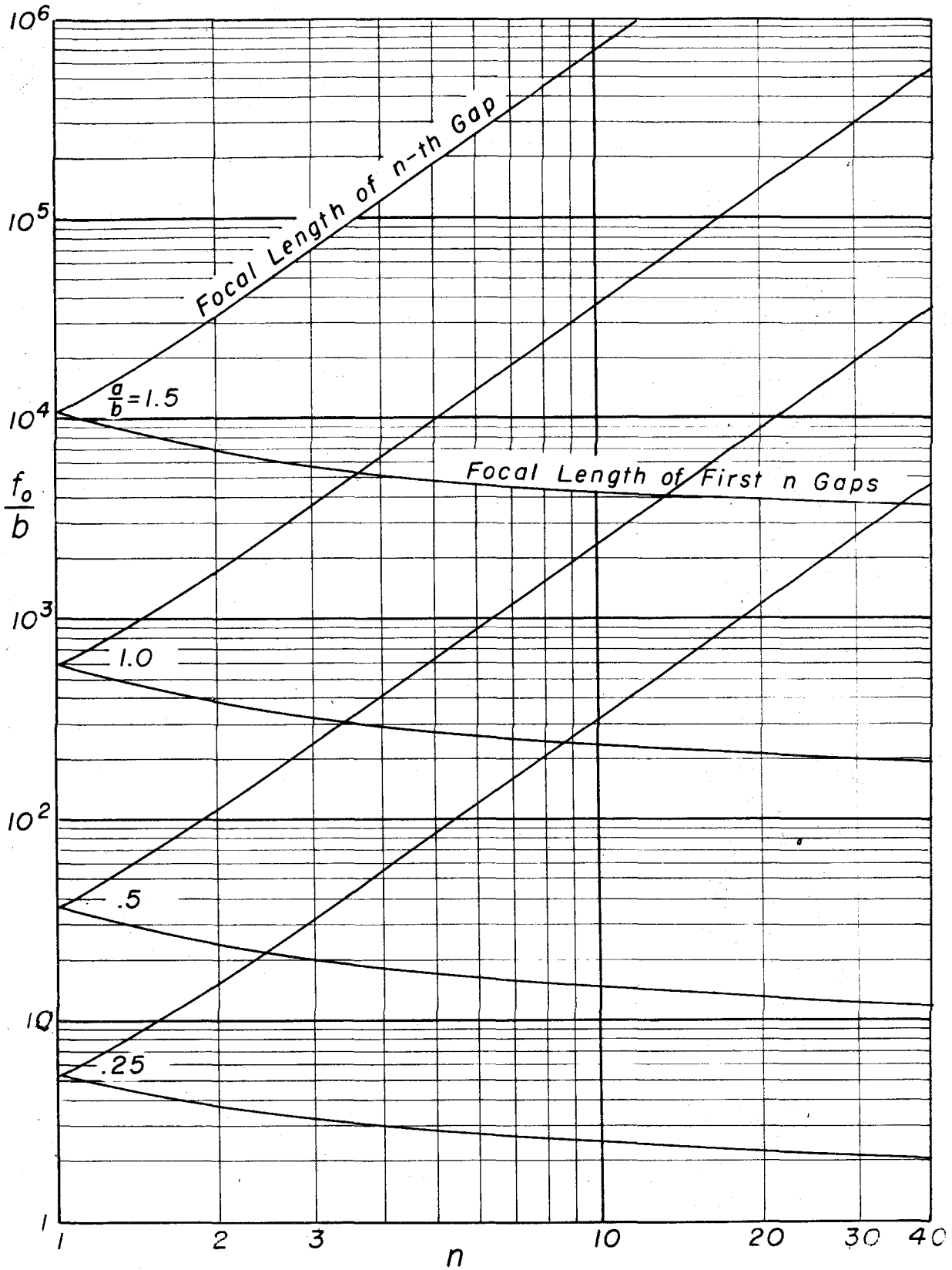

Fig. 17 FOCAL PROPERTIES OF A MULTI-CYLINDER ACCELERATING COLUMN

The object side focal length f_o is plotted for a column having cylinders of length b and radius a, with the first cylinder voltage equal to the potential difference between cylinders.

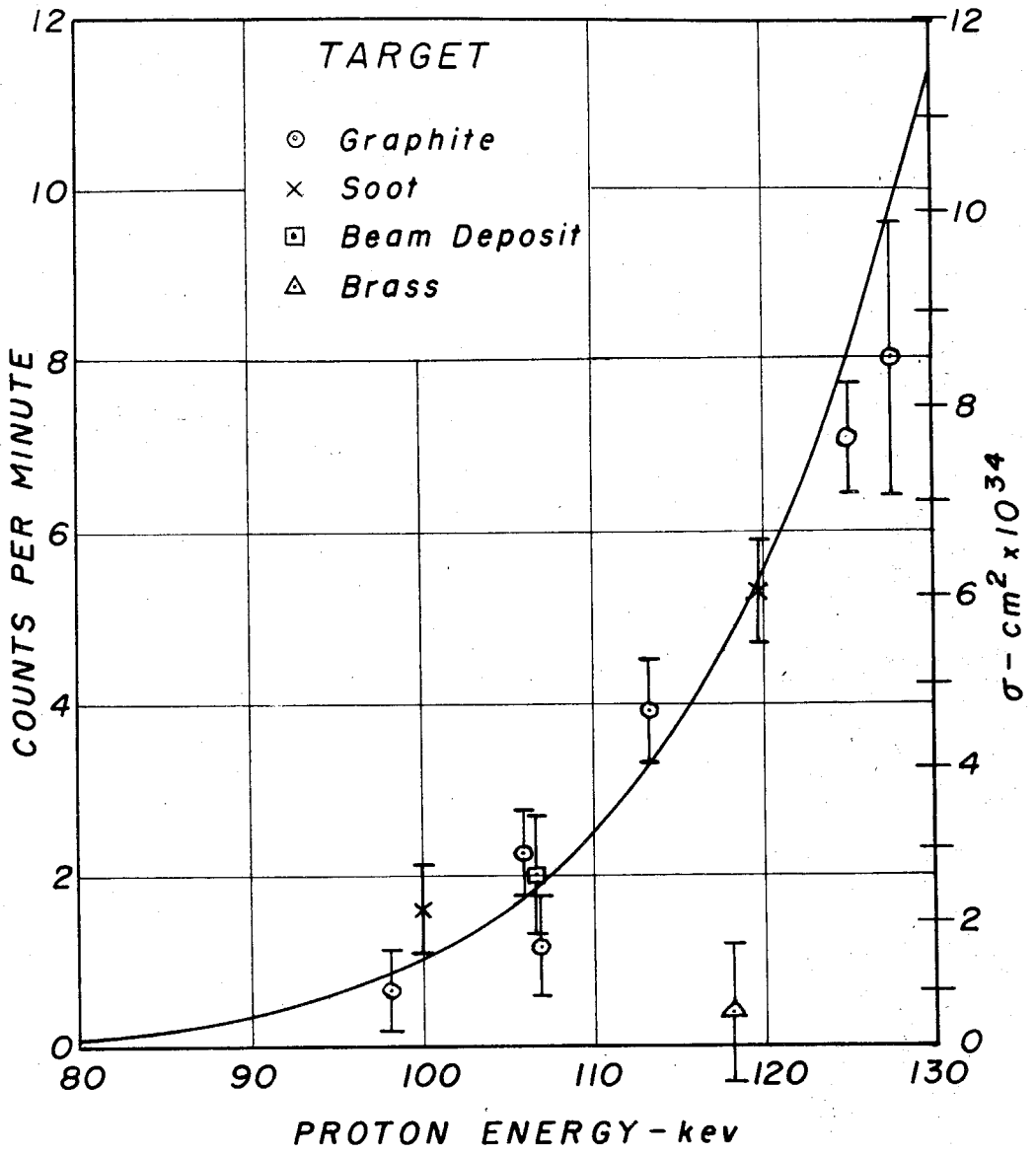

Fig. 18 YIELD CURVE FROM $C^{12}(p\gamma,e^+)C^{13}$

The thick target activity data is plotted for various target materials. The ordinate on the left is the initial counting rate which would be measured by the counter after an infinite bombarding period with a 100 μa proton beam. The curve drawn through the points is proportional to the calculated thick target yield given by equation 77-2. The corresponding capture cross-section is indicated at the right.

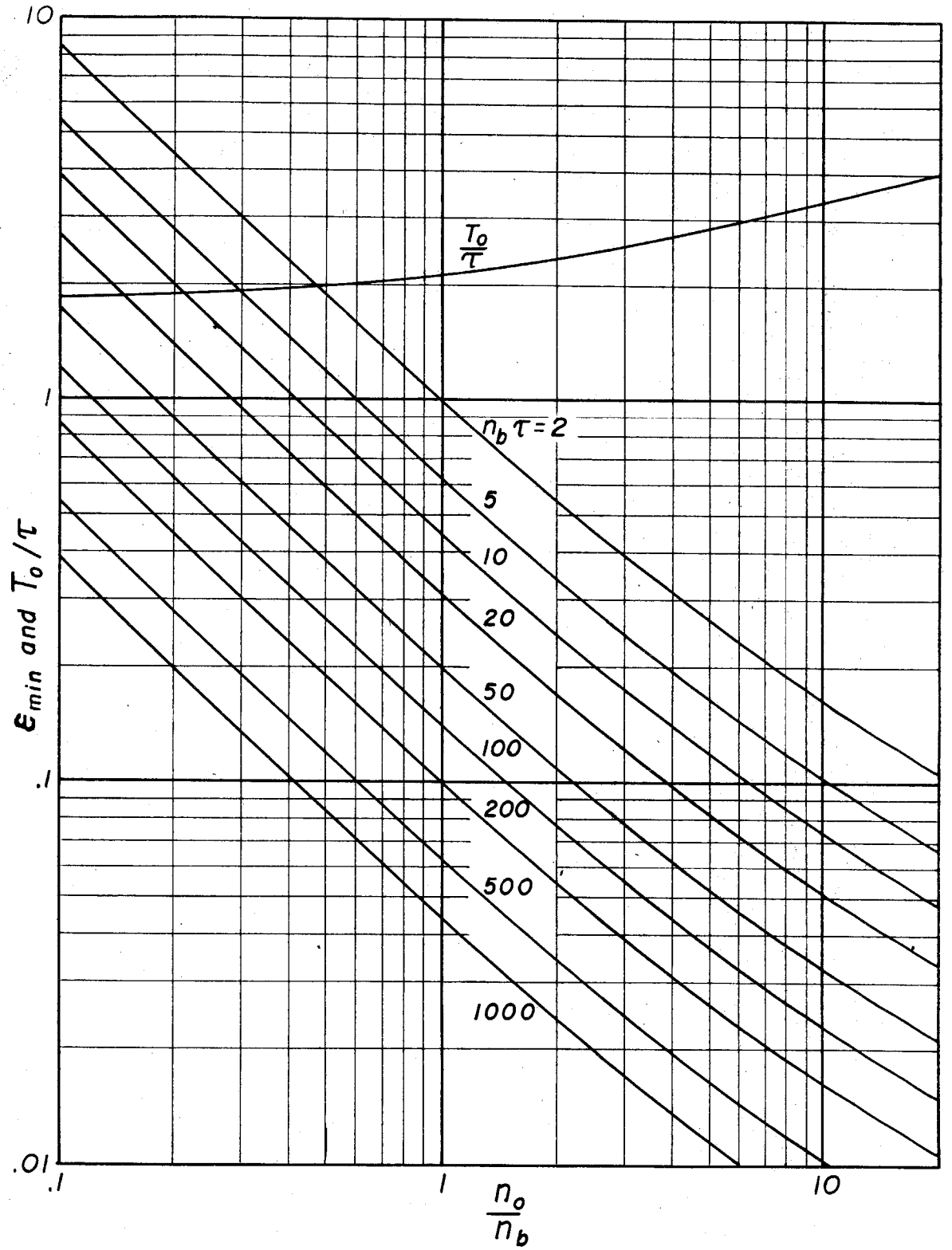

Fig. 19 STATISTICAL ERRORS FROM AN EXPONENTIAL DECAY RATE

T_o is the counting time which gives minimum error for an exponential decay rate $n = n_o \exp([t \log 2]/\tau)$ of half-life τ in the presence of a background of n_b counts per unit time. The corresponding minimum probable error ε_{min} is given for various background count rates.

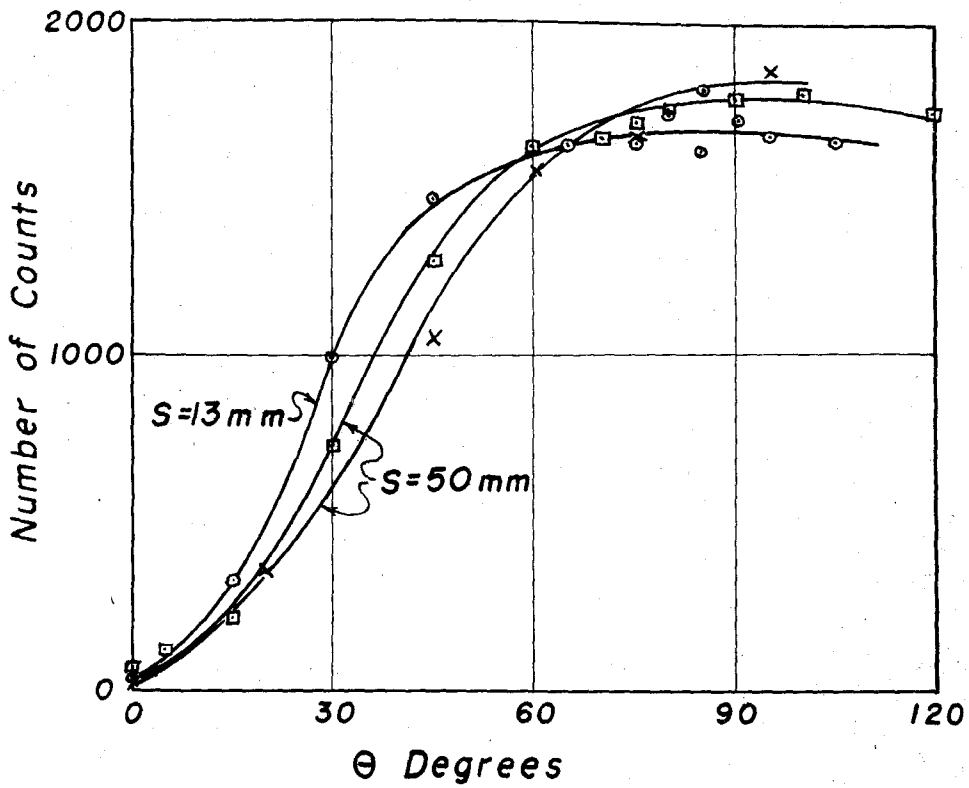

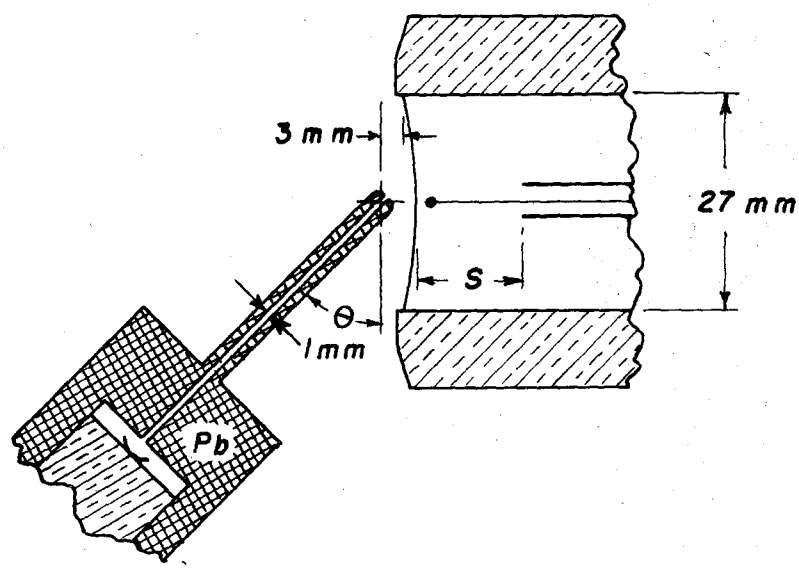

Fig. 20 MEASUREMENT OF COUNTING EFFICIENCY

The sensitivity of mica-window beta-ray counters was explored with a collimated beam of Ra D beta particles. The special low background counter used in measuring the N^{13} activity had 13 mm of exposed central wire. Sensitivity curves for two standard counters having 50 mm of exposed wire are shown for comparison.

BIBLIOGRAPHY

1) E. S. Lamar, W. W. Buechner and R. J. van de Graaff.
"The Production of Proton Beams."
J. App. Phys. 12, 132 (1941)

2) E. S. Lamar and W. W. Buechner.
"Ion Beams in High Voltage Tubes Using Differential Pumping."
J. App. Phys. 18, 22 (1947)

3) J. G. Trump and R. J. van de Graaff.
"Insulation of High Voltages in Vacuum."
J. App. Phys. 18, 327 (1947)

4) L. S. Goddard.
"Optical Characteristics of a Two-Cylinder Electrostatic Lens."
Camb. Phil. Soc. Proc. 42, 106 (1946)

5) Zworykin, Morton, Ramberg, Hillier and Vance.
"Electron Optics and the Electron Microscope."
John Wiley and Sons, inc. 1945

6) J. D. Cockroft and E. T. S. Walton.
"Experiments with High Velocity Positive Ions."
Proc. Roy. Soc. A129, 477 (1930)

7) Oliphant and Rutherford.
"Experiments on the Transmutation of Elements by Protons."
Proc. Roy. Soc. A141, 259 (1933)

8) H. R. Crane, C. C. Lauritsen and A. Soltan.
"Artificial Production of Neutrons."
Phys. Rev. 45, 507 (1934)

9) E. S. Lamar and O. Luhr.
"A Convenient Proton Source."
Phys. Rev. 44, 947 (1933)

10) Tuve, Dahl and Hafstad.
"Production and Focusing of Intense Positive Ion Beams."
Phys. Rev. 48, 241 (1935)

11) W. H. Zinn.
"Low Voltage Positive Ion Source."
Phys. Rev. 52, 655 (1937)

Bibliography - continued

12) T. Jorgensen.
"A Study of Adjustments of a Zinn-Type Ion Source."
Rev. Sci. Inst. 19, 28 (1948)

13) Jennings, Swartz and Rossi.
"A Small Pressure-Insulated Electrostatic Generator."
Rev. Sci. Inst. 15, 64 (1944)

14) A. T. Finkelstein.
"A High Efficiency Ion Source."
Rev. Sci. Inst. 11, 94 (1940)

15) M. von Ardenne.
"Uber eine Atomumwandlungsanlage fur Spannungen bis zu 1 Million Volt."
Zeits. f. Phys. 121, 236 (1943)

16) Office of Naval Research, London Branch.
"Report on British Ion Sources."
Technical Report OANAR-48-47 (1948)

17) Rutherglen and Cole.
"A Radio-Frequency Ion Source with High Percentage Yield of Protons."
Nature, 160, 545 (1947)

18) J. A. Stratton
"Electromagnetic Theory." p 327
McGraw-Hill Book Company. 1941

19) W. V. Smith.
"Surface Recombination of H Atoms and OH Radicals."
J. Chem. Phys. 11, 110 (1943)

20) Loeb.
"Kinetic Theory of Gases." p 312
McGraw-Hill Book Company. 1927

21) Thompson and Headrick.
"Space-Charge Limitations on the Focus of Electron Beams."
I. R. E. 28, 318 (1940)

22) J. R. Pierce.
"Rectilinear Electron Flow in Beams."
J. App. Phys. 11, 548 (1940)

Bibliography - continued

23) Hansen and Webster.
"Electrostatic Focusing at Relativistic Speeds."
Rev. Sci. Inst. 7, 17 (1936)

24) H. A. Bethe.
"Energy Production in Stars."
Phys. Rev. 55, 434 (1939)

25) Fowler, Lauritsen and Lauritsen.
"Gamma-Radiation from Excited States of Light Nuclei."
Rev. Mod. Phys. 20, 236 (1948)

26) Siegbahn and Slatis.
"The Radiation from Active Nitrogen."
Arkiv. f. Ast. Math. Fys. 32A, No 9 (1945)

27) Livingston and Bethe.
"Nuclear Physics."
Rev. Mod. Phys. 9, 245 (1937)

28) R. B. Roberts and N. P. Heydenburg.
"Further Observations on Production of N^{13}."
Phys. Rev. 53, 374 (1938)